A Spectral Budget Model for the Longitudinal Turbulent Velocity in the Stable Atmospheric Surface Layer

TIRTHA BANERJEE*

Nicholas School of the Environment, Duke University, Durham, North Carolina

DAN LI

Program in Atmospheric and Oceanic Sciences, Princeton University, Princeton, New Jersey

JEHN-YIH JUANG

Department of Geography, National Taiwan University, Taipei, Taiwan

GABRIEL KATUL

Nicholas School of the Environment, and Department of Civil and Environmental Engineering, Duke University, Durham, North Carolina

(Manuscript received 4 March 2015, in final form 25 August 2015)

ABSTRACT

A spectral budget model is developed to describe the scaling behavior of the longitudinal turbulent velocity variance σ_u^2 with the stability parameter $\zeta = z/L$ and the normalized height z/δ in an idealized stably stratified atmospheric surface layer (ASL), where z is the height from the surface, L is the Obukhov length, and δ is the boundary layer height. The proposed framework employs Kolmogorov's hypothesis for describing the shape of the longitudinal velocity spectra in the inertial subrange, Heisenberg's eddy viscosity as a closure for the pressure redistribution and turbulent transfer terms, and the Monin–Obukhov similarity theory (MOST) scaling for linking the mean longitudinal velocity and temperature profiles to ζ. At a given friction velocity u_*, σ_u reduces with increasing ζ as expected. The model is consistent with the disputed z-less stratification when the stability correction function for momentum increases with increasing ζ linearly or as a power law with the exponent exceeding unity. For the Businger–Dyer stability correction function for momentum, which varies linearly with ζ, the limit of the z-less onset is $\zeta \approx 2$. The proposed framework explains why σ_u does not follow MOST scaling even when the mean velocity and temperature profiles may follow MOST in the ASL. It also explains how δ ceases to be a scaling variable in more strongly stable (although well-developed turbulent) ranges.

1. Introduction

The scaling laws of the root-mean-squared longitudinal turbulent velocity component σ_u normalized by the friction velocity u_* with distance z from a solid boundary has received renewed attention in meteorology and turbulence (Alfredsson et al. 2011; Smits and Marusic 2013; Poggi et al. 2006; Cai et al. 2008; Hsieh and Katul 2009; Hansen et al. 2012; McKeon 2013; Stevens et al. 2014; Yang et al. 2014). While it has been known for some time that σ_u/u_* in the atmospheric surface layer (ASL) deviates from the expectations set by the Monin and Obukhov similarity theory (MOST) even for near-neutral conditions (Bradshaw 1978; Kader and Yaglom 1990; Kaimal 1978; Kaimal and Finnigan 1994; Charuchittipan and Wilson 2009), MOST scaling for σ_u/u_* remains the "workhorse" model for practical problems because alternative scaling laws that retain the simplicity of MOST remain lacking (Zilitinkevich and Calanca 2000). The goal of this work is to offer a potential alternative to MOST for the stable ASL for "idealized" conditions. These idealized conditions

*Current affiliation: Atmospheric Environmental Research, Institute of Meteorology and Climate Research, Karlsruhe Institute of Technology, Garmisch-Partenkirchen, Germany.

Corresponding author address: Tirtha Banerjee, IMK-IFU, Karlsruhe Institute of Technology, Kreuzeckbahnstr. 19, 82467 Garmisch-Partenkirchen, Germany.
E-mail: tirtha.banerjee@kit.edu

DOI: 10.1175/JAS-D-15-0066.1

include stationary planar homogeneous flows in the absence of subsidence and well-developed turbulence so as to ensure an extensive inertial subrange spectrally separating production from viscous dissipation scales.

A universal logarithmic scaling with z, originally proposed by Townsend (1976) and expressed as $\sigma_u^2/u_*^2 = B_1 - A_1 \log(z/\delta)$ for neutral turbulent boundary layers, has been recently confirmed by different high Reynolds number laboratory experiments and large-eddy simulations (Marusic et al. 2013; McKeon 2013; Smits and Marusic 2013; Stevens et al. 2014), where the atmospheric boundary layer (ABL) height δ is featured as a significant dynamical variable. However, a satisfactory phenomenological theory predicting how σ_u^2/u_*^2 is altered by thermal stratification in idealized stably stratified ASL flows while recovering its well established near-neutral limit remains elusive and frames the scope here. By phenomenological theory, we mean a theory that relates a number of empirical observations on σ_u^2/u_*^2 in a way that is consistent with the fundamental equations but the theory itself is not directly derived from these fundamental equations. Hence, as a starting point for developing such a phenomenological theory, a number of observations and findings must be reviewed.

First, under near-neutral conditions and for an idealized ASL, the mean velocity U exhibits a logarithmic scaling with z roughly for the same range of z/δ as σ_u/u_*. The logarithmic scaling for the mean velocity is expressed as $U^+ = \kappa^{-1}\log(z^+) + C_w$, where κ is the von Kármán constant and C_w is a surface roughness coefficient, and $U^+ = U/u_*$ and $z^+ = u_* z/\nu$ are nondimensional velocity and length from the wall, respectively, and ν is the kinematic viscosity. Second, in the presence of thermal stratification, the mean velocity is reasonably described by incorporation of a stability correction function for momentum $\phi_m(\zeta)$ that is only a function of the stability parameter $\zeta = z/L$ according to MOST, where L is the Obukhov length and $\zeta < 0$ indicates unstable stratification and $\zeta > 0$ indicates stable stratification. Links between the energy spectrum of turbulence and $\phi_m(\zeta)$ (or similar measures) have received renewed interest in the last decade (Sukoriansky et al. 2006; Katul et al. 2011; Li et al. 2012b; Salesky et al. 2013; Sukoriansky and Galperin 2013; Katul et al. 2013, 2014; Li et al. 2015b) but will not be elaborated on here. Third, several studies reported measurements of spectra, cospectra of momentum and heat fluxes as well as the corresponding integral length scales, and their variations with the stability (Kaimal et al. 1972; Kaimal 1973; Caughey 1977; Högström 1990; Launiainen 1995; Canuto et al. 2008; Basu et al. 2014). This dependence of integral scales on ζ will be explicitly accommodated in the proposed spectral budget model. Fourth, a balance between the turbulent kinetic energy dissipation rate, mechanical production, and buoyant destruction (Wyngaard and Coté 1971; Katul et al. 2014) is often assumed though several datasets suggest the existence of a finite transport term that can vary with ζ as reviewed elsewhere (Salesky et al. 2013). Implications and biases due to a stability-dependent nonnegligible transport term will be discussed later in an appendix but not explicitly included at this stage. Last, it was noted by Wyngaard and Coté (1971), Nieuwstadt (1984), and Olesen et al. (1984) among others that all dimensionless parameters resulting from local combinations of flow variables reach a uniform value at sufficiently high ζ (but still maintaining a sufficiently developed turbulent state), thereby losing their z dependence. This phenomenon is referred to as z-less stratification, and its limit is generally assumed to be close to $\zeta \approx 1$ or 2 (Olesen et al. 1984). However, measurements of σ_u/u_*, compiled by Pahlow et al. (2001), suggest that a power-law scaling in ζ appears to be maintained even when $\zeta > 2$, which was used to argue against the z-less scaling for σ_u. The analysis of Pahlow et al. (2001) was problematic because of the presence of the so-called submesomotions. The revised analysis (Basu et al. 2006) of the same dataset (augmented with others) did not show such spurious behavior. The proposed spectral model will be used to partly clarify some (but not all) of the conditions promoting z-less stratification, including their connection to the shape of $\phi_m(\zeta)$.

The proposed framework builds on a previous spectral budget method developed to explain the logarithmic scaling exhibited by σ_u^2/u_*^2 when $\zeta = 0$ (Banerjee and Katul 2013). A later study expanded the spectral budget method to describe σ_u/u_* under unstable conditions (i.e., $\zeta < 0$) by the addition and appropriate modeling of a buoyant production term in the spectral budget (Banerjee et al. 2014). It has been found that z, δ, and L are all parameters required for describing the variation of σ_u/u_*. Analytical results for σ_u/u_* from the theory were also possible in two limiting conditions identified as $z/\delta < 0.02$ and $-\zeta < 0.5$ and $0.02 \ll z/\delta < 0.1$ and $-\zeta > 0.5$ (Banerjee et al. 2014). While progress has been made toward understanding several characteristics of σ_u/u_* in the unstable boundary layer, there has been limited progress for the stable atmospheric boundary layer (SABL), which is the main focus here. This lack of progress is partly experimental because contamination from nonturbulent phenomena such as gravity waves; drainage forces from change in terrain slope, low-level jets, and mesoscale motions; and passage of clouds during nocturnal conditions, which are known to impact σ_u, are ubiquitous in field experiments under stable conditions (Pahlow et al.

2001; Cava et al. 2004). Thus, the SABL is characterized by different levels of balance between mechanical production of turbulent kinetic energy (TKE) and buoyant damping under different conditions ranging from almost nonturbulent to well-mixed conditions (Ohya et al. 1997). In low wavenumbers, the effects of gravity waves dominate close to the Brunt–Väisälä frequency N and can influence the turbulent spectra and cospectra of the velocity component (Einaudi and Finnigan 1981; Finnigan and Einaudi 1981; Leyi and Panofsky 1983; Finnigan et al. 1984; Hunt et al. 1985; Rohr et al. 1988; Edwards and Mobbs 1997; Mahrt et al. 2001; Cava et al. 2004; Campos et al. 2009; Mahrt et al. 2012). Heat and pollutants can be transferred vertically by waves and low-frequency turbulent motions and a vertical diffusion length scale of σ_w/N for heat and pollutant transfer has also been identified where σ_w^2 is the vertical velocity variance (Hunt et al. 1985). Weinstock (1981) reported a strong correlation between the turbulent kinetic energy dissipation rate and σ_w. The proposed spectral budget here will not consider such nonstationarities, the role of gravity waves (and hence N), and intermittent switching between turbulent and nonturbulent states. The turbulence in the SABL is assumed to be sufficiently developed so that a sufficiently large separation between the integral length scale and the viscous dissipation length scale (or the Kolmogorov microscale) always exists and Kolmogorov's theory for the inertial subrange (Kolmogorov 1941) approximates velocity and temperature spectra for all scales bounded between the integral and Kolmogorov scales. This is consistent with the observation by Huang and Bou-Zeid (2013) that this "continuously turbulent SABL" is different from the "intermittently turbulent SABL." The continuously turbulent SABL is also described as "weakly stable" and is the subject of the present work while the intermittently turbulent SABL is often designated as a"very stable" boundary layer (Mahrt 1998; Huang and Bou-Zeid 2013). Approaches that analyzed similar problems where the spectrum of (vertical) velocity and temperature shift from waves at large scales (characterized by a −3 power law) to inertial at smaller scales (characterized by a −5/3 power law) are also not within the scope here and are reviewed elsewhere (Sukoriansky et al. 2006; Sukoriansky and Galperin 2013). The proposed derivation also does not require or assume any link between the turbulent kinetic energy dissipation rate and σ_w. However, the derivation here does assume that much of the turbulent kinetic energy resides in the longitudinal and lateral velocity components, which is plausible given that the damping effects of atmospheric stability are in the vertical direction.

2. Theory

a. Background and definitions

A coordinate system is defined with x, y, and z forming the longitudinal, lateral, and vertical directions, respectively. Standard Reynolds decomposition notation is also employed so that the longitudinal u, lateral v, and vertical w velocities are decomposed into a stationary mean and fluctuating or turbulent quantities using $u = U + u'$, $v = V + v'$, and $w = W + w'$ with $V = 0$ based on the choice of the coordinate system. Potential temperature and pressure are also decomposed into a mean (T and P) and turbulent fluctuations (T' and p'), respectively. As earlier noted, it is assumed that the flow is characterized by high Reynolds and Peclet numbers (negligible molecular viscosity and diffusivity compared to their turbulent counterpart), stationary $[\partial(\cdot)/\partial t = 0]$, planar homogeneous in the mean $[\partial(\cdot)/\partial x = \partial(\cdot)/\partial y = 0]$ and without subsidence ($W = 0$) or significant mean horizontal pressure gradient ($\partial P/\partial x = \partial P/\partial y = 0$) as common to MOST. When these assumptions are incorporated into the equations for mean horizontal velocity and mean temperature, they result in $d\overline{u'w'}/dz = 0$ and $d\overline{w'T'}/dz = 0$, where $\overline{u'w'}$ and $\overline{w'T'}$ are the momentum and sensible heat fluxes, respectively. Beyond ignoring molecular diffusion and viscosity, the high Reynolds and Peclet numbers are assumed to be sufficiently large so as to further suppress formation of gravity waves or laminarization of the flow. A large spectral separation is also assumed between the integral length scale of the flow and the Kolmogorov microscale so that scales bounded by these two limits maintain an approximate locally homogeneous and isotropic state as earlier noted.

b. The TKE budget

The TKE budget for such an idealized ASL can be written as

$$\frac{\partial e}{\partial t} = 0 = -\overline{u'w'}\frac{dU}{dz} + \beta\overline{w'T'} - \frac{\partial}{\partial z}\left[\frac{1}{2}\overline{w'(u'^2 + v'^2 + w'^2)} + \frac{1}{\rho}\overline{w'p'}\right] - \overline{\varepsilon}, \quad (1)$$

where $e = (1/2)(\sigma_u^2 + \sigma_v^2 + \sigma_w^2)$ is the TKE; $\sigma_u^2 = \overline{u'^2}$, $\sigma_v^2 = \overline{v'^2}$, and $\sigma_w^2 = \overline{w'^2}$; $\beta = g/T$ is the buoyancy parameter; g is the gravitational acceleration; ρ is the mean air density; t denotes time and $\overline{\varepsilon}$ is the mean TKE dissipation rate; and T denotes potential temperature. The first, second, and third terms on the right-hand side (RHS) of Eq. (1) are the mechanical production and buoyant destruction of TKE (written as positive as per convention;

note that $\overline{w'T'}$ would be negative for a stable atmosphere) and the transport of TKE by turbulence and pressure–velocity interactions, respectively. For several ASL applications, the production, buoyant, and dissipation terms can exist in a near balance (Townsend 1976; Pope 2000; Wilson 2008). However, some datasets demonstrated that the transport term cannot be neglected, especially in stable stratification, and the imbalance in the TKE budget is suggested to vary with the stability parameter $\zeta = z/L$ (Salesky et al. 2013). A consequence of this imbalance on the σ_u scaling will be explored separately in appendix A but this imbalance is momentarily ignored. In case of a TKE balance (i.e., negligible transport), MOST (Monin and Obukhov 1954) yields $dU/dz = \phi_m(\zeta)u_*/(\kappa z)$ and $\overline{\varepsilon} = [\phi_m(\zeta) - (\zeta)]u_*^3/(\kappa z)$, where $L = -u_*^3/(\kappa\beta\overline{w'T'})$ and $\phi_m(\zeta)$ is the stability correction function for momentum as mentioned earlier. In case the transport terms are significant, $\overline{\varepsilon}$ can be modified as $\overline{\varepsilon} = [\beta_2(\zeta) + \phi_m(\zeta) - (\zeta)]u_*^3/(\kappa z)$ following Salesky et al. (2013), where $\beta_2(\zeta)$ is a function of ζ that may be determined from experimental datasets.

Other common quantities are now defined. The flux Richardson number R_f is given by the ratio of the buoyant destruction rate of TKE $\beta\overline{w'T'}$ to the mechanical production rate of TKE $-P_m$:

$$R_f = \frac{\beta\overline{w'T'}}{-P_m} \tag{2}$$

and the gradient Richardson number R_g is given as

$$R_g = \frac{\beta\Gamma}{S^2}, \tag{3}$$

where $P_m = -S\overline{u'w'}$, $S = dU/dz = \phi_m u_*/(\kappa z)$ is the mean velocity gradient, and $\Gamma = dT/dz = \phi_T T_*/(\kappa z)$ is the mean potential temperature gradient. The u_* is, as before, the friction velocity defined as $-u_*^2 = \overline{u'w'}$ and T_* is defined as $T_* = u_*^2/(\kappa\beta L)$. Using these definitions, the flux Richardson number can be related to ζ using

$$R_f = \frac{\beta\overline{w'T'}}{S\overline{u'w'}} = \frac{\beta\overline{w'T'}}{-u_*^3\phi_m(\zeta)/(\kappa z)} = \frac{\zeta}{\phi_m(\zeta)}. \tag{4}$$

Unless otherwise mentioned, $\phi_m(\zeta)$ can be described by the widely used empirical Businger–Dyer (Businger and Yaglom 1971; Dyer 1974) form: $\phi_m(\zeta) = (1 + 4.7\zeta)$ for $0 < \zeta < 2$, which is the range of stability conditions explored here. This is commensurate with the critical flux Richardson number ($R_f = 0.2$, same for the gradient Richardson number R_g as well) for the applicability of local similarity theory since when $\zeta = z/L = 2$, $R_f = \zeta/\phi_m = 0.2$ (Grachev et al. 2013). The concomitant temperature stability correction function ϕ_T is also assumed to be given by its MOST representation as $\phi_T = 0.74 + 4.7\zeta$. To a leading order, $\phi_m(\zeta) \approx \phi_T(\zeta)$, though for $R_g > 0.1$, this approximation no longer holds (Zilitinkevich et al. 2013; Katul et al. 2014). With this background, the spectral budget for TKE and its connection to σ_u are presented.

3. A spectral budget formulation for TKE

At an arbitrary wavenumber k defined along the longitudinal direction, the spectral budget can be expressed as (Hinze 1959; Panchev 1971; Banerjee et al. 2014)

$$\overline{\varepsilon} = -\frac{d\overline{U}}{dz}\int_k^\infty F_{wu}(s)\,ds + \frac{g}{T}\int_k^\infty F_{wT}(s)\,ds + F(k) + 2\nu\int_0^k s^2 E_{\text{tke}}(s)\,ds, \tag{5}$$

where the first, second, third, and fourth terms on the RHS represent the mechanical production and buoyant destruction of TKE in the range of $[k, \infty]$, the transfer of TKE in the range $[k, \infty]$, and the viscous dissipation in the range of $[0, k]$, respectively. It is to be noted that the formulation here assumes that $\overline{\varepsilon} > 0$. The mechanical generation term $-d\overline{U}/dz\int_k^\infty F_{wu}(s)\,ds$ is also positive and as buoyancy acts against mechanical generation of turbulence, the term $(g/T)\int_k^\infty F_{wT}(s)\,ds$ would be negative for the SABL. The transfer and viscous dissipation terms are defined with a positive sign. If k tends to 0 without the presence of any buoyancy term, $\overline{\varepsilon} = -d\overline{U}/dz\int_0^\infty F_{wu}(s)\,ds$ and $\int_0^\infty F_{wu}(s)\,ds = \overline{u'w'}$. The sign of $\overline{u'w'}$ is negative so the production term is always positive here. Similarly, the normalizing property $\int_0^\infty F_{wT}(s)\,ds = \overline{w'T'} < 0$ owing to $\overline{w'T'} < 0$ in the SABL. Using the Heisenberg model, for all eddies between the wavenumbers 0 and k, the action of smaller eddies can be represented by an additional viscosity, since the way in which these smaller eddies transfer momentum is similar to the action of ordinary friction. This additional viscosity must depend upon the intensity of the small eddies—on the part of the spectrum with large wavenumbers by means of a certain integral that was formulated based on dimensional arguments by Heisenberg (1948). Using this argument, the transfer term can be "closed" as

$$F(k) = \nu_t(k)\overline{|\text{curl}(\tilde{u})|^2} \approx 2\nu_t(k)\int_0^k s^2 E_{\text{tke}}(s)\,ds, \tag{6}$$

where $\nu_t(k)$ is a the wavenumber-dependent Heisenberg viscosity. With this simplification, the spectral budget Eq. (5) becomes (Banerjee et al. 2014)

$$\overline{\varepsilon} = -\frac{dU}{dz}\int_k^\infty F_{wu}(s)\,ds + 2[\nu_t(k)+\nu]\int_0^k s^2 E_{\text{tke}}(s)\,ds + \frac{g}{T}\int_k^\infty F_{wT}(s)\,ds. \quad (7)$$

a. Modeling the mechanical production term

To link the spectral budget to MOST scaling, it is assumed that $k_a = 1/[\gamma(\zeta)z]$ within the ASL, where $\gamma(\zeta)$ varies with ζ and is specified later. The $\gamma(\zeta)z$ represents a stability-dependent crossover between the large scales and the inertial scales, which may be related to the integral length scale of the flow but is not necessarily identical to it. The reduction of γ with stability from a neutral limit magnitude of unity implies that the extent of the inertial subrange reduces with increasing ζ.

Thus for a wavenumber k that satisfies $k\gamma(\zeta)z > 1$, the traditional inertial subrange scaling applies (Kolmogorov 1941) so that

$$E_{\text{tke}}(k) = C_o\overline{\varepsilon}^{2/3}k^{-5/3}, \quad (8)$$

where $C_o = (33/55)C_K$ is the Kolmogorov constant when k is interpreted as a one-dimensional cut along the longitudinal direction and $C_K = 1.55$ is the Kolmogorov constant associated with three-dimensional wavenumbers. The 33/55 coefficient originates from a 1D interpretation (along x) of the TKE spectrum that is locally homogeneous and isotropic given by $E_{\text{tke}}(k) = (1/2)[E_u(k) + E_v(k) + E_w(k)]$, with $33/55 = (18/55 + 24/55 + 24/55)/2 = (66/2)/55$ since the Kolmogorov spectral constants for the individual one-dimensional velocity spectra are $(18/55)C_K$, $(24/55)C_K$, and $(24/55)C_K$, respectively (Banerjee and Katul 2013). In conventional turbulence literature where index notation is prevalent, $E_{\text{tke}}(k)$ is equivalent to the $E_{e1}(k_1) = (1/2)[E_{11}(k_1) + E_{22}(k_1) + E_{33}(k_1)]$ as discussed by Pope (2000), where k_1 is the wavenumber along the longitudinal direction and $E_{11}(k_1)$, $E_{22}(k_1)$, and $E_{33}(k_1)$ are component velocity spectra along the longitudinal, lateral, and vertical directions, respectively. Throughout, meteorological notation is employed unless otherwise stated, and k is interpreted as k_1 as noted before for notational simplicity.

Using the cospectral budget formulation provided by Katul et al. (2014), the following form can be derived for $k > k_a$:

$$F_{wu}(k) = C_{uw}\overline{\varepsilon}^{1/3}Sk^{-7/3}, \quad (9)$$

which is in agreement with the accepted "−7/3" scaling for the cospectra of momentum flux in the inertial subrange (Lumley 1967), where $C_{uw} = (2C_o)/(5A_u)$, and $A_u \approx 1.8$ is the Rotta constant. Hence, the production term in the spectral budget [Eq. (7)] can be simplified by substituting $\overline{\varepsilon}$ in Eq. (9) with $\overline{\varepsilon} = [\beta_2(\zeta) + \phi_m(\zeta) - \zeta]u_*^3/(\kappa z)$, as well as setting $\beta_2(\zeta) = 0$ to yield

$$\frac{dU}{dz}\int_{k_a}^\infty F_{wu}(s)\,ds = \left(\frac{\phi_m u_*}{\kappa z}\right)\left[\frac{2}{5}\frac{C_o}{A_u}\frac{(\phi_m-\zeta)^{1/3}u_*}{(\kappa z)^{1/3}}\right]\left(\frac{\phi_m u_*}{\kappa z}\right)\left(\frac{3}{4}k_a^{-4/3}\right) = \frac{u_*^3}{z}\frac{2}{5}\frac{3}{4}\frac{C_o}{A_u}\frac{\phi_m^2(\phi_m-\zeta)^{1/3}}{\kappa^{7/3}}\gamma^{4/3}. \quad (10)$$

b. Modeling the buoyant destruction term

Using the cospectral budget formulation for $F_{wT}(k)$ provided in Katul et al. (2014), the following form can be derived for $k > k_a$:

$$F_{wT}(k) = C_{wT}\overline{\varepsilon}^{1/3}\Gamma k^{-7/3}, \quad (11)$$

where $C_{wT} = (2C_oQ)/5A_T$, $A_T \approx 1.8$ is the Rotta constant for heat assumed to be the same as its momentum counterpart (equal to A_u) here, and $Q(\zeta)$ varies with ζ as follows:

$$Q = 1 + \frac{\beta C_T N_T}{(1-C_{1T})C_o\Gamma\overline{\varepsilon}}, \quad (12)$$

where $C_T \approx 0.8$ is the Kolmogorov–Obukov–Corrsin constant for the temperature spectrum in the inertial subrange (along x), $C_{1T} = 3/5$ is a constant associated with the isotropization of the production term in the cospectral budget of temperature flux and can be predicted from rapid distortion theory (RDT) for isotropic turbulence, and N_T is the thermal variance dissipation rate defined as

$$N_T = \overline{w'T'}\Gamma = -\frac{1}{\beta}R_f\Gamma P_m = -\frac{\zeta\Gamma S u_*^2}{\phi_m\beta}. \quad (13)$$

Hence, Q can be simplified as

$$Q = 1 - \frac{\beta C_T}{(1-C_{1T})C_o\Gamma u_*^3(\phi_m-\zeta)/(\kappa z)}\frac{\zeta\Gamma u_*^3\phi_m}{\phi_m\beta\kappa z} = 1 - \frac{C_T\zeta}{(1-C_{1T})C_o(\phi_m-\zeta)}. \quad (14)$$

It is interesting to note that $Q(\zeta) \approx C_{wT}/C_{uw} < 1$ is consistent with the findings from the Kansas experiment (Kaimal and Finnigan 1994). Because $C_{wT} \approx C_{uw}Q(\zeta)$, the buoyant destruction term in the spectral budget [Eq. (7)] can be simplified as

$$\frac{g}{T}\int_{k_a}^{\infty} F_{wT}(s)\,ds = \left(\frac{g}{T}\right)\left[\frac{2}{5}\frac{C_o}{A_T}\frac{(\phi_m-\zeta)^{1/3}u_*}{(\kappa z)^{1/3}}\right]\left(\frac{u_*^2}{\kappa\beta L}\right)\left(\frac{\phi_T}{\kappa z}\right)Q\left(\frac{3}{4}k_a^{-4/3}\right) = \frac{u_*^3}{z}\frac{2}{5}\frac{3}{4}\frac{C_o}{A_T}\frac{\phi_T\zeta Q(\phi_m-\zeta)^{1/3}}{\kappa^{7/3}}\gamma^{4/3}. \quad (15)$$

c. Spectral budget at $k_a = 1/(\gamma z)$

The spectral budget equation can now be used to find the spectral form of $E_{\text{tke}}(k)$ (which is later linked to σ_u^2) in the range 0–k_a using the modeled forms of the mechanical production and buoyant destruction terms. It is necessary to recast the spectral budget equation [Eq. (7)] in the following form:

$$\overline{\varepsilon} - \frac{d\overline{U}}{dz}\int_{k_a}^{\infty} F_{wu}(s)\,ds + \frac{g}{T}\int_{k_a}^{\infty} F_{wT}(s)\,ds = 2[\nu_t(k)]\int_0^{k_a} s^2 E_{\text{tke}}(s)\,ds, \quad (16)$$

where it is assumed that $\nu_t \gg \nu$, that is, the turbulent viscosity is much higher than the molecular viscosity for high Reynolds number flows. Using Eqs. (10) and (15), Eq. (16) is rewritten as

$$2[\nu_t(k)]\int_0^{k_a} s^2 E_{\text{tke}}(s)\,ds = \frac{u_*^3}{z}\left[\frac{\phi_m-\zeta}{\kappa} - \frac{2}{5}\frac{3}{4}\frac{C_o}{A_u}\frac{\phi_m^2(\phi_m-\zeta)^{1/3}}{\kappa^{7/3}}\gamma^{4/3} + \frac{2}{5}\frac{3}{4}\frac{C_o}{A_T}\frac{\phi_T\zeta Q(\phi_m-\zeta)^{1/3}}{\kappa^{7/3}}\gamma^{4/3}\right]. \quad (17)$$

Assuming $E_{\text{tke}}(k)$ is inertial for k bounded by $[k_a, \infty]$ given by Kolmogorov's theory (i.e., ignoring exponential cutoff due viscous effects at high k), ν_t can be determined as (Banerjee et al. 2014)

$$\nu_t(k_a) = \frac{3C_H C_o^{1/2}\overline{\varepsilon}^{1/3}}{4k_a^{4/3}}, \quad (18)$$

where C_H is the Heisenberg constant defined as $C_H = (8/9)C_o^{-3/2}$. Substituting the definition of $\nu_t(k)$ from Eq. (18), Eq. (17) can be written as

$$\int_0^{k_a} s^2 E_{\text{tke}}(s)\,ds = \frac{u_*^2}{z^2}\frac{2}{3C_H C_o^{1/2}}\left[\frac{(\phi_m-\zeta)^{2/3}}{\kappa^{2/3}\gamma^{4/3}} - \frac{2}{5}\frac{3}{4}\frac{C_o}{A_u}\frac{\phi_m^2}{\kappa^2} + \frac{2}{5}\frac{3}{4}\frac{C_o}{A_T}\frac{\phi_T\zeta Q}{\kappa^2}\right], \quad (19)$$

which is consistent with Banerjee et al. (2014):

$$\int_0^{k_a} s^2 E_{\text{tke}}(s)\,ds = \frac{u_*^2}{z^2}C_{\text{st}}, \quad (20)$$

where C_{st} here is defined as

$$C_{\text{st}}(\zeta) = \frac{2}{3C_H C_o^{1/2}}\left[\frac{(\phi_m-\zeta)^{2/3}}{\kappa^{2/3}\gamma^{4/3}} - \frac{2}{5}\frac{3}{4}\frac{C_o}{A_u}\frac{\phi_m^2}{\kappa^2} + \frac{2}{5}\frac{3}{4}\frac{C_o}{A_T}\frac{\phi_T\zeta Q}{\kappa^2}\right]. \quad (21)$$

In the neutral limit, $\zeta = 0$, $\phi_m = 1$, $\phi_T \approx 1$, and $\gamma = 1$, thus recovering C_{st} to be

$$C_{\text{st-neutral}} = \frac{2}{3C_H C_o^{1/2}}\left(\frac{1}{\kappa^{2/3}} - \frac{2}{5}\frac{3}{4}\frac{C_o}{A_u}\frac{1}{\kappa^2}\right). \quad (22)$$

With appropriate values of the constants [$C_H \approx 1$, $C_o = (33/55)1.55$, $\kappa = 0.4$, and $A_u = 1.8$], yields a $C_{\text{st-neutral}} \approx 0.56$.

The function $\gamma(\zeta)$ is now discussed. As earlier noted, the integral length scale decreases with increasing ζ (Kaimal et al. 1972; Kaimal 1973; Caughey 1977; Högström 1990; Launiainen 1995; Canuto et al. 2008). While γz is not identical to the integral length scale as earlier noted, its dependence on ζ is assumed to follow a similar pattern. For this purpose, $\gamma(\zeta) \approx (1 + a_L\zeta)^{-1}$ so as to ensure a $\gamma(0) = 1$, where a_L is a decay coefficient. Possible decay rates of γ with increasing ζ are discussed and are shown in Fig. 1.

The variations of the integral length scale of the longitudinal velocity normalized by z are shown as black circles on Fig. 1, which were computed by Salesky et al. (2013) using the Advection Horizontal Array Turbulence Study (AHATS) data collected in the ASL. A good fit to this data is $a_L = 3$. The dashed–dotted line refers to the integral length scale of the vertical velocity whose functional form has been computed from the Kansas experiment as $(0.55 + \zeta)^{-1}$ (Kaimal and Finnigan 1994). It is to be noted that its neutral limit is greater than 1, which indicates a larger length scale at lower k than z. However, when normalized by this neutral limit, it can also be used as a guide to how the breakpoint wavenumber in the spectrum representing the crossover from large to inertial subrange scales shifts to higher wavenumbers with increasing stability. In addition, because the integral length scale of the vertical velocity is closely aligned with this breakpoint, it may be better suited for approximating γz than the integral length scale of the longitudinal velocity. As evident from Fig. 1, its variation is quite similar to the variation of the integral length scale

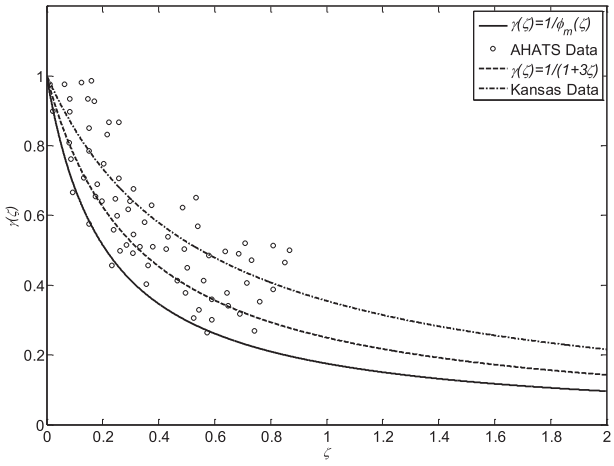

FIG. 1. Variation of $\gamma(\zeta)$ with the stability parameter $\zeta = z/L$. Black circles show the normalized integral length scale for vertical turbulent velocity from AHATS data. The dashed line indicates a fit to AHATS data as $\gamma = 1/(1 + 3\zeta)$. The dashed–dotted line represents the normalized integral length scale for vertical turbulent velocity from the Kansas experiment. The black line indicates $\gamma(\zeta) = 1/\phi_m(\zeta)$, where ϕ_m is the stability correction function for momentum determined from the Kansas experiment.

of the longitudinal velocity. Interestingly, $\gamma(\zeta) \approx 1/\phi_m(\zeta)$ is also shown for reference and appears to be also similar to the one inferred from the integral length scale of the vertical velocity. For this reason, this aforementioned form is used for analytical tractability. Notwithstanding which precise approximation to use, it appears that a value of a_L in the range from 3 to 4.7 is reasonable.

d. Formulation for C_{st}: Numerical fitting

To proceed with an analytical derivation, the integral expressed in Eq. (20) must be simplified. Figure 2 shows the variation of the function C_{st} with ζ. As observed, C_{st} suggests the possible existence of a two-regime formulation somewhat similar to the result of Banerjee et al. (2014). In zone I, C_{st} is roughly flat until $\zeta = 0.1$, assuming the neutral limit of $C_{st-neutral} = 0.56$, which is designated as $c = 0.56$. In zone II, C_{st} can be described by an approximate power law of the form $C_{st} = a\zeta^b$, where a and b can be obtained by a numerical curve fitting as $a \approx 2.966$ and $b \approx 0.66$ with a coefficient of determination of 0.99. Although a smooth transition between the two regimes (zone I and zone II) can be possibly formulated by an interpolation scheme, it is assumed that $\zeta \approx 0.1$ is the location of this transition for all practical purposes. With this two-part formulation for C_{st}, the shape of the $E_{tke}(k)$ can now be inferred for each regime in the limit $0 - k_a$.

e. Formulation for zone I

Since the form of E_{tke} in the limit 0–k_a is unknown, it may be assumed to be a power law; that is,

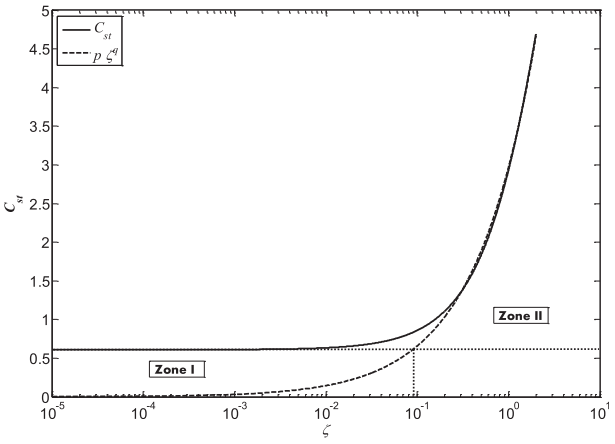

FIG. 2. Variation of C_{st} with the stability parameter $\zeta = z/L$. Zones I and II are marked and the transition between the two zones is at $\zeta \approx 0.1$. In zone I C_{st} is nearly constant but follows a power law in zone II.

$$E_{tke}(k)_{0-k_a} = rk^l. \tag{23}$$

Substituting this power-law expression in Eq. (20), the following identity can be derived:

$$\left(\frac{r}{3+l}\gamma^{-3-l}\right)z^{-3-l} = (u_*^2 c)z^{-2}. \tag{24}$$

Equating terms in the left-hand side (LHS) and RHS of Eq. (24), one can obtain

$$l = -1 \quad \text{and} \quad r = 2u_*^2 c\gamma^2, \tag{25}$$

while the parameter $c = C_{st-neutral} = 0.56$ is known a priori as discussed earlier.

Thus to summarize, for zone I,

$$E_{tke}(k) = \begin{cases} C'_{tke}u_*^2 k^{-1}, & \text{if} \quad k\gamma z \le 1 \\ C_o\bar{\varepsilon}^{2/3}k^{-5/3}, & \text{otherwise} \end{cases}, \tag{26}$$

where $C'_{tke} = 2c\gamma^2$. Thus the E_{tke} spectrum recovers the much-discussed k^{-1} scaling as reviewed elsewhere (Banerjee et al. 2014). Furthermore, it can also be assumed that the k^{-1} scaling is valid until $kH = 1$, where H is a measure of the size of largest turbulent eddies in the SABL and the spectrum is flat at lower wavenumbers; that is, $E_{tke} = C'_{tke}u_*^2(1/H)^{-1}$ form continuity requirement at $kH = 1$.

f. Formulation for zone II

Following the same approach presented in the previous subsection, E_{tke} is assumed to be a power law; that is,

$$E_{tke}(k)_{0-k_a} = pk^q. \tag{27}$$

Substituting this general power-law expression in Eq. (20), the following identity can be derived:

$$\left(\frac{p}{3+q}\gamma^{-3-q}\right)z^{-3-q} = \left(\frac{u_*^2 a}{L^b}\right)z^{b-2}. \tag{28}$$

Equating terms in the LHS and RHS of Eq. (28), one can obtain

$$q = -1-b \quad \text{and} \quad p = \frac{u_*^2 a(2-b)}{L^b}\gamma^{2-b}, \tag{29}$$

where a and b are known a priori from C_{st}. It is interesting to note that $q = -1-b \approx -1.67 \approx -5/3$, which indicates that the E_{tke} spectrum follows a scaling law analogous to its inertial value at higher ζ. Because of the similarity in the spectral exponents and to ensure spectral continuity, we simply extend the inertial subrange spectrum up to some scale $k\gamma_1(\zeta)z$, where γ_1 is discussed later. However, it must be emphasized that the main mechanisms leading to the approximate $-5/3$ scaling here differ from those in the inertial subrange. For maintaining maximum simplicity here, the $E_{tke}(k)$ spectrum can be described as

$$E_{tke}(k) = \begin{cases} 0, & \text{if } k\gamma_1 z \le 1 \\ C_o\overline{\varepsilon}^{2/3}k^{-5/3}, & \text{otherwise} \end{cases}. \tag{30}$$

Now the determination of γ_1 is discussed. It is known that the turbulent (but not necessarily the total) kinetic energy in σ_u is quite suppressed and eddies are appreciably deformed by stratification at eddy sizes much larger than the Ozmidov length scale $L_0 = (\overline{\varepsilon}/N^3)^{1/2}$, where $N = [(g/T)(dT/dz)]^{1/2}$. At these large scales, nonturbulent phenomena such as gravity waves become energetically prevalent but the turbulent contribution to the energy is small (or negligible). For the idealized ASL considered here where $\zeta > 0.1$, $L_0/(\kappa z) \sim \{[\phi_m(\zeta) - \zeta]^{1/2}[\zeta\phi_T(\zeta)]^{-3/4}\}$. To a first order, the $L_0/(\kappa z)$ declines at a rate commensurate with $[\phi_m(\zeta)]^{-1}$ when setting $\phi_T(\zeta) \sim \phi_m(\zeta) \sim \zeta$ and $[\phi_m(\zeta) - \zeta] \sim \zeta$. An assumption of maximum simplicity again is that the turbulent component of the kinetic energy spectrum lacks significant energy at $k\gamma_1(\zeta)z \le 1$ with $\gamma_1(\zeta)$ declining with ζ at a rate commensurate with $\gamma(\zeta)$. However, instead of determining γ_1 from L_0, it will be determined so as to ensure continuity between zones I and II when deriving σ_u^2, as will be discussed later. Another interesting observation is that the spectrum exhibits an apparent inertial signature in its exponent ($=-5/3$) at higher stability. Given that the spectrum is also found to follow $-5/3$ scaling at highly unstable conditions (Banerjee et al. 2014), it can be stated that the signature of buoyancy is an apparent "inertialization" or transition to an approximate $-5/3$ scaling from a combination of $-5/3$ and -1 scalings dominating the E_{tke} spectrum for near-neutral conditions.

g. Linking the longitudinal velocity variance to TKE

For neutral and unstable atmospheric surface layers, it was argued elsewhere (Basu et al. 2010; Banerjee and Katul 2013; Banerjee et al. 2014) that $\sigma_u^2 \approx \sigma_v^2 + \sigma_w^2$ and thus $e = (1/2)(\sigma_u^2 + \sigma_v^2 + \sigma_w^2) \approx (1/2)(\sigma_u^2 + \sigma_u^2) \approx \sigma_u^2$. It is assumed that this condition is also valid for stable conditions, especially at high Reynolds and Peclet numbers when turbulence is well separated from gravity waves. To test this assumption, experimental data (described in detail in section 4) collected over two distinct vegetation canopies at the Duke forest over 4 yr are used. Figure 3 demonstrates a one-to-one comparison between σ_u^2 and e for two different seasons (i.e., summer and winter) and for two different vegetation canopies: a second growth oak–hickory hardwood (HW) forest and a loblolly (PI) plantation. In all cases it can be assumed that $\sigma_u^2 \approx e$ irrespective of surface cover and stability parameters (the slopes are 0.80, 0.84, 0.70, and 0.76 for winter pine, summer pine, winter HW, and summer HW, respectively). Thus the TKE spectrum can be integrated to obtain σ_u^2 for the purposes here.

h. The longitudinal velocity variance

Integrating the $E_{tke}(k)$ spectra from the formulation for zone I [Eq. (26)] to obtain the longitudinal velocity variance results in

$$\sigma_u^2 = \int_0^{1/H} C'_{tke}u_*^2(1/H)^{-1}\,ds + \int_{1/H}^{k_a} C'_{tke}u_*^2 s^{-1}\,ds + \int_{k_a}^{\infty} C_o\varepsilon^{2/3}s^{-5/3}\,ds. \tag{31}$$

Assuming $H = \gamma\delta$ and substituting the values from Eq. (26), Eq. (31) becomes

$$\frac{\sigma_u^2}{u_*^2} = 2c\gamma^2 - 2c\gamma^2\log\left(\frac{z}{\delta}\right) + \frac{3}{2}\frac{C_o}{\kappa^{2/3}}(\phi_m - \zeta)^{2/3}\gamma^{2/3}, \tag{32}$$

which can also be written in a form consistent with Townsend's attached eddy hypothesis as

$$\frac{\sigma_u^2}{u_*^2} = B_1 - A_1\log\left(\frac{z}{\delta}\right), \tag{33}$$

where

$$B_1 = \frac{3}{2}\frac{C_o}{\kappa^{2/3}}(\phi_m - \zeta)^{2/3}\gamma^{2/3} + 2c\gamma^2 \tag{34}$$

and

$$A_1 = 2c\gamma^2, \tag{35}$$

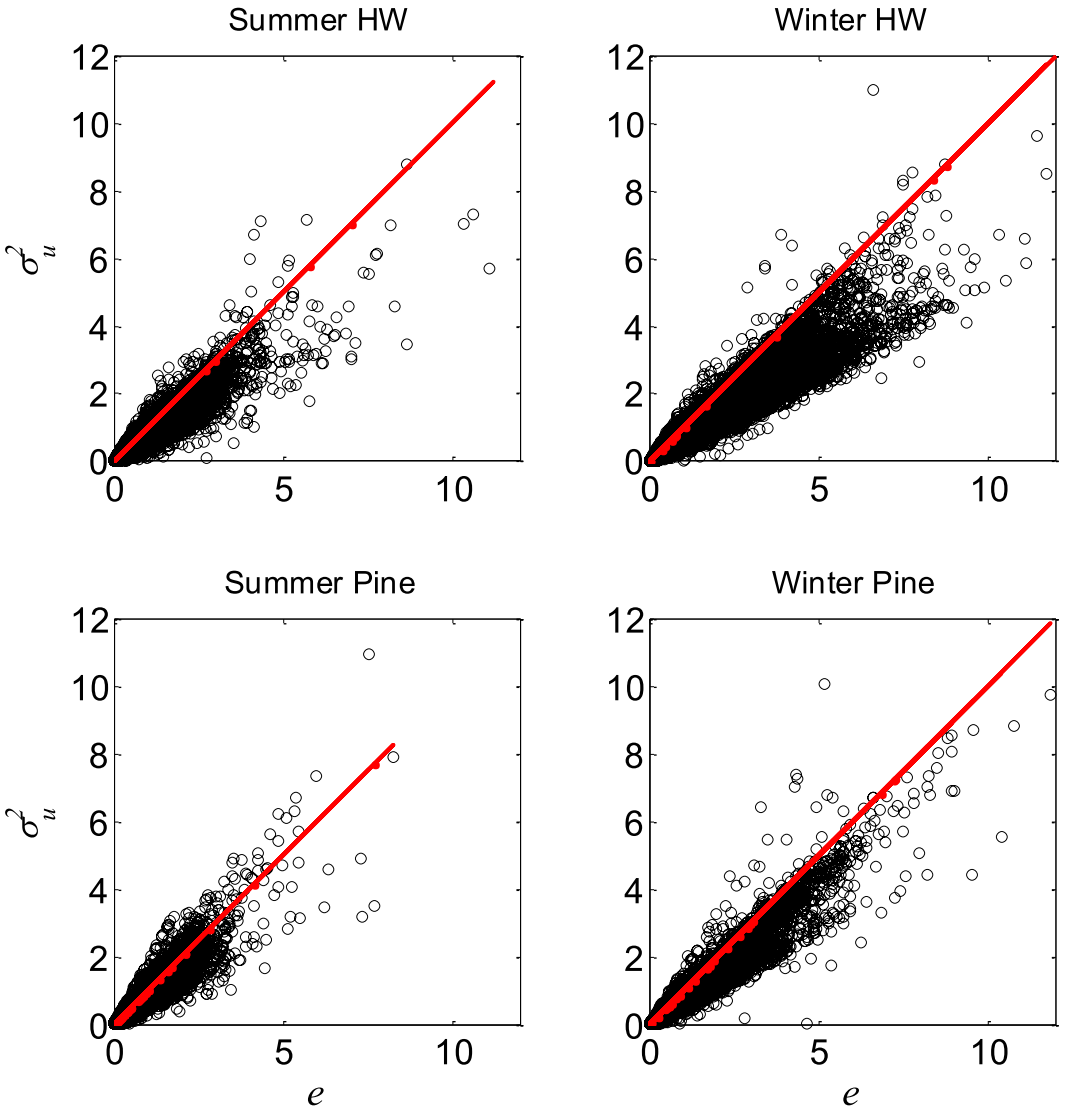

FIG. 3. Comparison between the turbulent kinetic energy e and σ_u^2 for pine and hardwood canopies for two different seasons: summer and winter. The slopes are 0.80 (winter, pine), 0.70 (winter, HW), 0.76 (summer, HW), and 0.84 (summer, pine).

where $\gamma = \gamma(\zeta)$ and thus the Townsend parameters now vary (mildly) with stability for near-neutral to slightly stable conditions.

If the second formulation for zone II is used, the $E_{\text{tke}}(k)$ can be integrated to derive the longitudinal velocity variance as

$$\frac{\sigma_u^2}{u_*^2} = \frac{3}{2}\frac{C_o}{\kappa^{2/3}}(\phi_m - \zeta)^{2/3}\gamma_1^{2/3}. \tag{36}$$

It is also interesting to note that the boundary layer height is not present in the formulation for zone II, which indicates that at higher stability σ_u is no longer sensitive to the boundary layer height (as expected). The parameter γ_1 can be found out by imposing continuity condition on σ_u^2/u_*^2 at $\zeta = 0.1$ (i.e., the transition between the two formulations). Equating Eqs. (32) and (36) at $\zeta = 0.1$, γ_1 can be calculated to have a near-neutral limit $\gamma_1 \approx 1$ and can be assumed to reduce with stability somewhat similar to $\gamma(\zeta)$. Again for simplicity, we choose $\gamma_1(\zeta) \approx 1/\phi_m(\zeta)$ based on the scaling argument that the Ozmidov length scale L_o decreases with increasing stability as $1/\phi_m(\zeta)$. Unfortunately, this continuity constraint results in weak scale separation between all the key length scales here—L_0, z, L, and δ (at least when compared to zone I). Given the number of assumptions used to separate the two formulations and the associated uncertainties, predictions based on

the formulation for zone I and zone II are separately compared to data for all ζ and biases are then analyzed as will be shown in section 5 and appendix B. Both formulations predict the correct neutral limit of σ_u/u_* (between 2 and 3).

The onset of z-less scaling in σ_u/u_* can now be assessed by inserting the estimate of $\gamma_1(\zeta) \approx 1/\phi_m(\zeta)$ into Eq. (36) and rearranging to yield

$$\frac{\sigma_u^2}{u_*^2} = \frac{3}{2}\frac{C_o}{\kappa^{2/3}}\left[1 - \frac{\zeta}{\phi_m(\zeta)}\right]^{2/3}. \tag{37}$$

Evidently, for $\zeta \ll 1$, $\phi_m(\zeta) \approx 1$ and z-less scaling is assured for the σ_u/u_* formulation derived in zone II. However, the onset of z-less scaling for stability regimes where $\zeta > 1$ is of interest here. As ζ increases, z-less scaling in σ_u/u_* appears to be recovered from Eq. (37) if $\phi_m(\zeta)$ increases at rate much faster than ζ so that $\zeta/\phi_m(\zeta) \ll 1$. Conversely, absence of z-less scaling can arise when $\phi_m(\zeta)$ increases at rate slower than ζ. It can be surmised that z-less scaling in σ_u/u_* is dependent on whether $\zeta/\phi_m(\zeta)$ becomes small compared to unity or simply independent of ζ with progressively increasing ζ. For the Kansas experiments, $\phi_m(\zeta) = 1 + 5\zeta$ for the SABL so that $\zeta/\phi_m(\zeta) \to 1/5$, a constant at large ζ, and is suggestive of possible z-less scaling in σ_u/u_*.

4. Datasets

To evaluate the model, four datasets are used. One dataset is a published laboratory experiment (Ohya et al. 1997) where the data sources are published figures digitized by us, one is an experiment over a large lake, and two datasets are from long-term monitoring initiatives above a pine (PI) plantation and a HW forest. The forest experiments are separated into summer and winter seasons to reflect large and small leaf area index (LAI) values.

The laboratory experiment was conducted by Ohya et al. (1997) in a wind tunnel where stably stratified flows were generated by cooling the aluminum floor to 3°C and maintaining the ambient air at 50°C. The experimental runs covered a range of u_* from 0.013 to 0.13 m s^{-1}, varying over an order of magnitude. The boundary layer height was measured and a range $0.1 < z/\delta < 0.5$ was reported in their results. Further details on the experiments and datasets can be found in Ohya et al. (1997).

The lake data include 20-Hz eddy covariance measurements of three-dimensional velocity and air temperature at four different heights (1.65, 2.30, 2.95, and 3.60 m) above an extensive lake surface. Details about the lake data and quality control measures can be found elsewhere (Vercauteren et al. 2008; Huwald et al. 2009; Li and Bou-Zeid 2011; Li et al. 2012a). In particular, the averaging interval is 30 min and data with fluxes measured at the four heights differing by more than 10% are excluded so as to maintain the constant flux assumption required by the derivation here and MOST scaling for mean velocity and temperature (Li et al. 2015a). The stability range covered in the lake measurements are mildly stable conditions ($\zeta = 0.001 - 0.25$). As a result, although the boundary layer heights are not measured in the experiments, they are expected to be not very low (on the order of hundreds of meters). Figure 4 shows the variations of u_* with ζ in the lake data. It is clear that the u_* decreases with increasing stability, which is expected. Interestingly, the decrease of u_* is captured by $\gamma(\zeta)$ with $a_L = 3$ (the black line) and $a_L = 4.7$ (the red line), as shown in Fig. 4. Note that $u_{*\text{neu}}$ indicates the neutral $u_* = 0.21$ m s^{-1}. This approach of multiplying the neutral u_* with $1/\gamma(\zeta)$ can also be used to capture the variation of u_* for comparison with the laboratory data as well in absence of explicit u_* for each run.

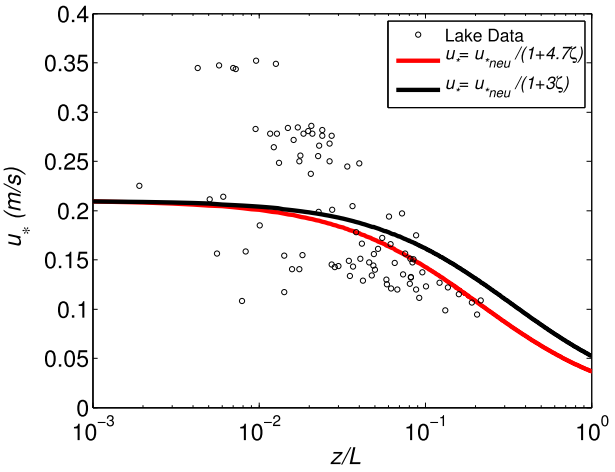

FIG. 4. Variations of u_* with $\zeta = z/L$ in the lake data. Under neutral conditions $u_{*\text{neu}}$ is the u_* (=0.21 m s^{-1}).

The forest experiments were conducted over two different but adjacent vegetation canopies: a loblolly pine plantation and a 100-yr-old second-growth oak hickory hardwood forest. The data include 10-Hz eddy covariance measurements of three-dimensional velocity and air temperature and the details of the experiments can be found elsewhere (Juang et al. 2008; Katul et al. 2012). The data span over 4 yr and are divided into summer and winter seasons. Since the experiments were conducted over the canopy, the $\zeta = z/L$ is modified as $\zeta = (z - d)/L$, where d is the zero-plane displacement height. This d is set to be zero in winter for the HW canopy and set to be $(2/3)h_c$ otherwise for both forests, where h_c is the canopy height ($h_c = 33$ m for HW and

$h_c = 15$ m for PI). The height of measurement z is 39.5 m for the HW and 15.5 m for the PI sites. The PI forest had a LAI varying from 2.65 to 4.56 $m^2 m^{-2}$ and the HW forest had a maximum LAI about 6 $m^2 m^{-2}$. The stability covered by this dataset ranges from mildly stable to highly stable conditions ($\zeta = 0.0001$–10). The u_* also varies with stability with modal values of 0.06 m s^{-1} in the summer and 0.35 m s^{-1} in the winter for both hardwood and pine canopies. The two forests were also collocated so they were subjected to similar meteorological conditions. There are 11 449 and 14 977 30-min runs for the PI site in the summer and winter, respectively. For the HW, there are 13 049 and 15 045 30-min runs in the summer and winter, respectively. To assess the applicability of MOST in the canopy sub layer (CSL), which is roughly 2–3 times h_c, some of the stored high-frequency data above the pine forest are used for illustration. The second-order structure function D_{uu} for u is calculated independently, which is regressed with $C_u\overline{\varepsilon}^{2/3}r^{2/3}$ where $C_u \approx 2$ (Stull 1988) and r is the lag in meters in the longitudinal direction (computed by multiplying the sampling time interval with the mean velocity using Taylor's frozen turbulence hypothesis). Within the inertial subrange, $D_{uu} = C_u\overline{\varepsilon}^{2/3}r^{2/3}$. It is found that the r range where this is true is approximately between 0.3 and 3 m. From this regression, the dissipation rate $\overline{\varepsilon}$ is computed. The mechanical $[-\overline{u'w'}dU/dz = u_*^3/(\kappa z)\phi_m]$ and buoyant destruction terms $[(g/T)\overline{w'T'}]$ in the TKE budget are then calculated using the dataset assuming MOST is valid in the CSL. If the independently computed production and dissipation rates are in balance, it suggests that MOST may be used in the canopy sublayer and that the TKE budget is, to reasonable approximation, represented by a balance between production and dissipation terms. Figure 5 shows a one-to-one comparison between production and dissipation terms for the high-frequency PI data collected over 12 different days for near-neutral and more stable conditions shown in black and red symbols, respectively. Overall, the terms are reasonably balanced suggesting that MOST may be applied to relevant mean-flow quantities in the CSL.

The boundary layer height was not measured in these experiments, either. However, since the dataset covers highly stable conditions, δ can be expected to drop significantly. On the other hand, δ was assumed not to appreciably exceed the average neutral ABL height of about 1000 m. This limit was determined from separate measurements in neutral conditions by Salesky et al. (2013). To have a realistic measure of δ at stable conditions, Zilitinkevich's model (Zilitinkevich 1972) is invoked. It is estimated that $\delta \approx \lambda\sqrt{(R/\mu)}$, where $R \approx 10$ is a constant (Zilitinkevich 1972), $\lambda = \kappa u_*/f$, $\mu = \lambda/L$,

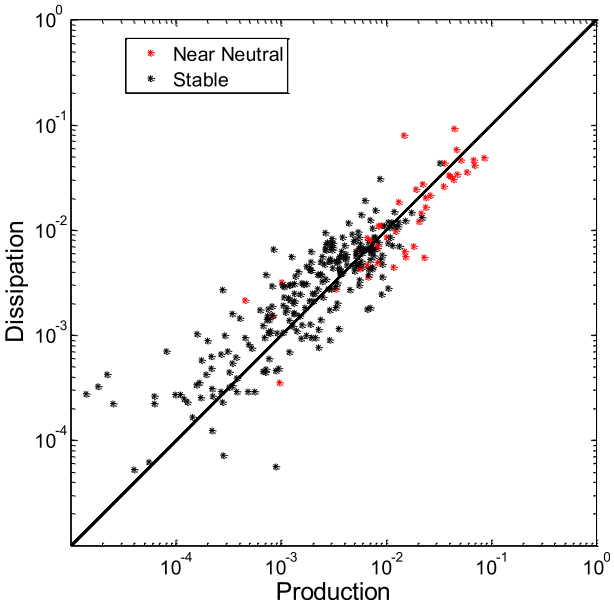

FIG. 5. Comparisons between production and dissipation terms in the TKE budget from pine data collected in the Duke forest over 12 days. Only stable stratifications are shown; near-neutral conditions are shown in red and more stable conditions are shown in black.

and $f = 10^{-4}$ rad s^{-1} is the Coriolis parameter. Using this approximation, it is estimated that $\delta \approx 50$ m under highly stable conditions. As a more improved estimation over the model of Zilitinkevich (1972), another model by Arya (1981) is used and is given by $\delta = au_*/f$, where $a \approx 0.3$. However, this modification is not found to impact the results significantly. Thus, these four datasets provide a wide range of conditions in terms of u_*, stability, and roughness (smooth: wind tunnel and lake experiments; very rough: forest experiments) to assess the proposed model.

5. Results and comparisons

a. *Evaluation of the model for σ_u*

Although two regimes have been identified for the formulation of σ_u, we first answer the following question: to what extent can the formulation for zone I (mildly stable regime) explain the experiments? The performance of the formulation for zone II will be explored later. Recall that the formulation for zone I recovers Townsend's form and explains how the Townsend parameters evolve with ζ, which is why exploring this formulation for the entire dataset is of interest. Figure 6 shows the comparison with the wind tunnel experiment conducted by Ohya et al. (1997), where σ_u is plotted against R_g. It is to be noted that the

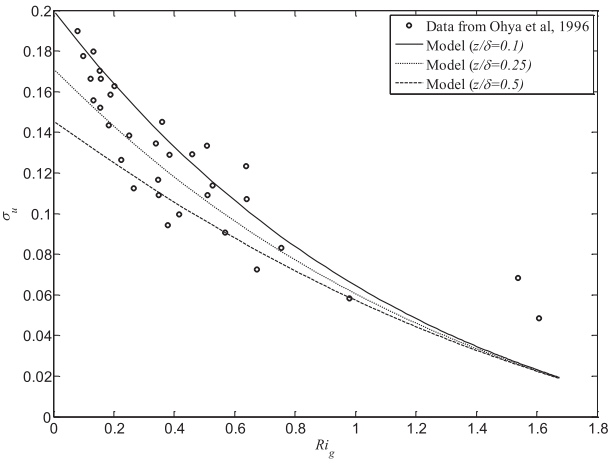

FIG. 6. Variations of σ_u with R_g from the laboratory experiment and from the model.

gradient Richardson number R_g can be rewritten in terms of the stability parameter $\zeta = z/L$ as $R_g = \zeta[\phi_T(\zeta)/\phi_m(\zeta)^2]$ (Kaimal and Finnigan 1994). Three different z/δ ratios, 0.1, 0.25, and 0.5, are used in order to cover the data and the comparisons are satisfactory. To cover the range of u_* (0.013–0.13) reported in Ohya et al. (1997), u_* is made dynamic by multiplying $u_{*\text{neu}}$ by $\gamma(\zeta)$ guided by Fig. 4.

For the lake data, the range of ζ covered by the lake data spans from 0.001 to 0.025, as shown in Fig. 4, and hence the boundary layer height is estimated not to be small under such mildly stable conditions (recall that the boundary layer height is not measured). Figure 7 shows the comparison between modeled and measured σ_u for the lake data when δ is calculated based on the model by Arya (1981) as discussed in section 4. As can be seen, the calculated δ decreases with increasing z/L from about 1000 m (under near-neutral conditions) to about 100 m under mildly stable conditions. Interestingly, the calculated δ from Arya's model over the lake does not change significantly when $z/L > 0.1$. However, it is noted that using a variable δ is not appreciably better when compared to calculations with a constant $\delta = 500$ and $\delta = 1000$ m.

Figure 8 shows the comparison with field data collected over the two forests. In Fig. 8, all panels show the comparison between measured and modeled (including MOST scaling) σ_u in terms of their variations with ζ. Ensemble averages of measured and modeled σ_u are shown and their variability is represented by black and red error bars, respectively. As expected, σ_u (in dimensional form) is found to reduce with stability, since the effects of mechanical turbulence is diminished by the effects of buoyancy. Figure 8a (summer, HW), Fig. 8d (winter, HW), Fig. 8g (summer, PI), and Fig. 8j (winter, PI) show the aforementioned comparisons with a preset boundary layer height $\delta = 50$ m since the data were mostly collected at night time when the boundary layer height is reduced to great extent. For $\delta = 50$ m, the comparisons are found to be satisfactory given that the ensemble averages almost follow each other. There is some unavoidable scatter in the data when they are observed at the low stability regime. However, instrument signal-to-noise ratio is also lower under very stable conditions and cannot be discarded. Figures 8b, 8e, 8h, and 8k in the middle column show these comparisons with a $\delta = 1000$ m, which is about the height of the ABL under mildly stable to near-neutral conditions (Stull 1988). With $\delta = 1000$ m, the model overestimates σ_u at low stabilities. Figures 8c, 8f, 8i, and 8l show the comparisons between measured and modeled σ_u from MOST, which is given as $\sigma_u = 2.5u_*$ (Stull 1988). As

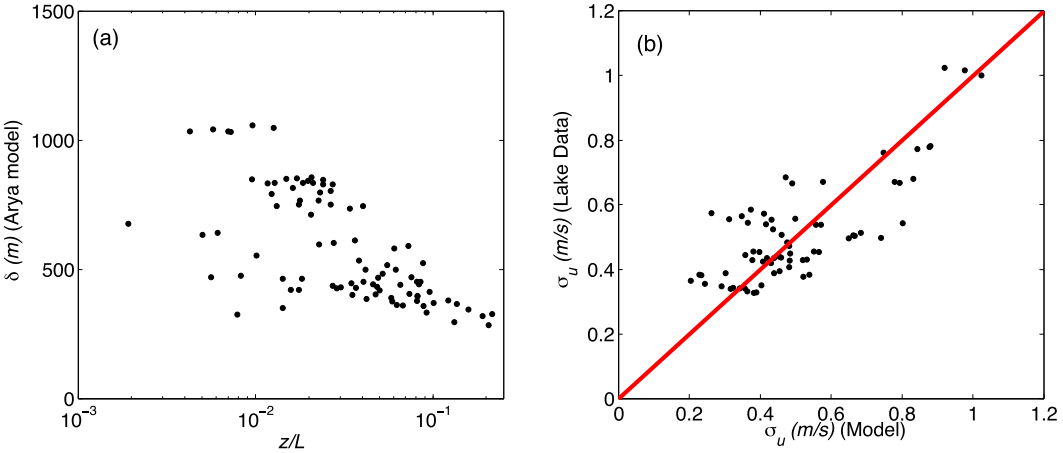

FIG. 7. (b) Comparison between measured and modeled σ_u for the lake experiment with δ computed from Arya's model ($R^2 = 0.61$). (a) The variation of the calculated boundary layer height.

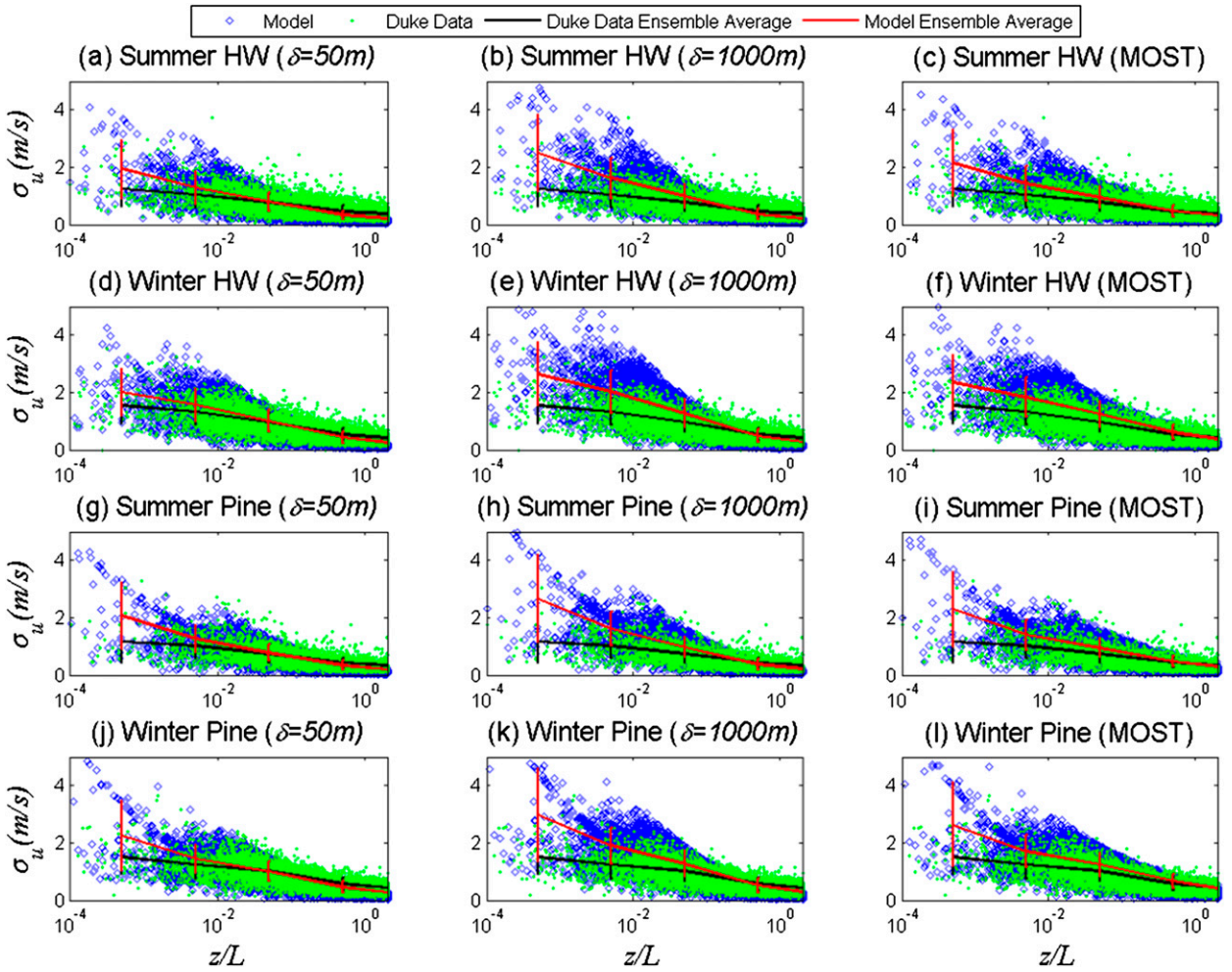

FIG. 8. Variations of σ_u with $\zeta = z/L$ from the forest experiments and from the model using the formulation for (left),(middle) zone I and (right) MOST. The comparisons are shown for two different canopies (pine and hardwood) and two different seasons (summer and winter) as indicated by the titles of the panels.

shown, MOST predictions often overestimate the data. Figure 9 demonstrates this feature better in which all panels show one to one comparisons between the modeled (x axis) (proposed model and MOST) and measured (y axis) σ_u. As described before, the comparisons with $\delta = 50$ m (Figs. 9a–d) are satisfactory but the proposed model here overestimates the data with a $\delta = 1000$ m (Figs. 9e, f). One important point to note for Figs. 7 and 8 is that the measured u_* for each data point is used to drive the model since u_* varies appreciably.

Since the forest dataset spans over such a wide range of stability conditions, the comparisons with the formulation for zone II are also shown in Fig. 10. Figure 10a (summer, HW), Fig. 10c (winter, HW), Fig. 10e (summer, PI), and Fig. 10g (winter, PI) show one-to-one comparisons between the modeled and measured σ_u. Figure 10b (summer, hardwood), Fig. 10d (winter, hardwood), Fig. 10f (summer, pine), and Fig. 10h (winter, pine) show variations of σ_u with ζ. Both one-to-one comparisons and variations with ζ show that σ_u is also reasonably captured by the formulation for zone II. However, it is again stressed that the boundary layer height is not present in the formulation for zone II, which is different from the formulation for zone I. The errors and biases in the predictions using both formulations for the complete range of stability are discussed in the appendix B. The main finding is that both model formulations are not particularly biased when comparisons are conducted separately for $\zeta < 0.1$ and $\zeta > 0.1$, presumably because of the fact that the γ_1 value is derived by matching the two formulations at $\zeta = 0.1$. Hence, in the zone-II formulation, $C_{st} \approx 0.6$ for $\zeta < 0.1$ instead of an asymptote to 0 (because of a zero additive parameter). Also, the fact that $(z - d)/\delta$ becomes on the

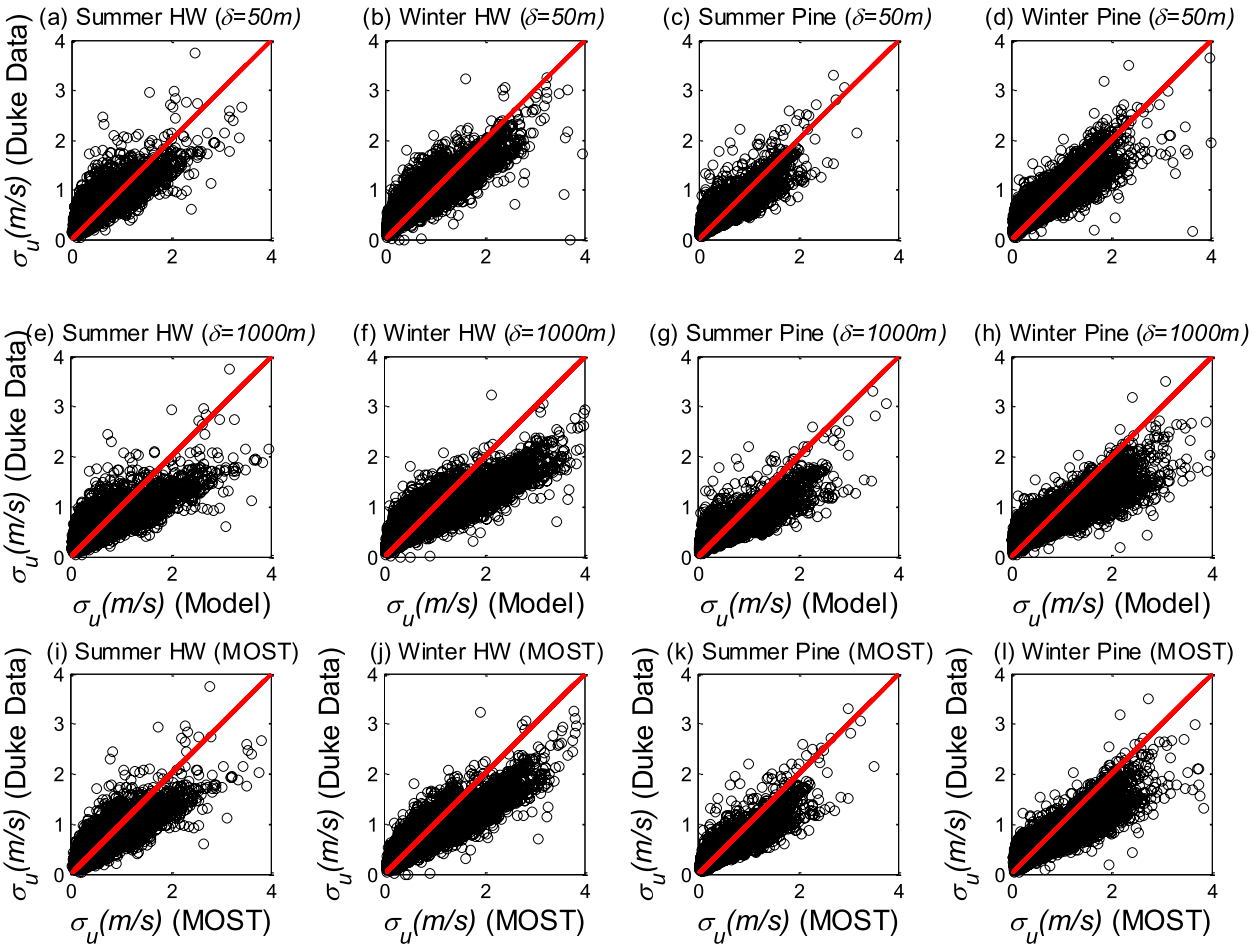

FIG. 9. Comparisons between measured and modeled σ_u using the formulation for (top), (middle) zone I and (bottom) MOST for the forest experiment. The comparisons are shown for two different canopies (pine and hardwood) and two different seasons (summer and winter) as indicated by the titles of the panels.

order of 0.5 means that the B_1 term becomes dominant (instead of A_1) for $\zeta > 0.1$ in the zone-I formulation. A consequence of this outcome is that the effects of δ also become muted in the zone-I formulation.

b. *Scaling variables*

An important point to be stressed in Fig. 8 is that the measured and modeled dimensionless quantity σ_u/u_* is not compared. Rather, σ_u is compared directly to avoid the known problem of self-correlation (Hicks 1978, 1981; De Bruin 1982; Pahlow et al. 2001; Andreas and Hicks 2002; Hartogensis and De Bruin 2005; Cava et al. 2008; Banerjee et al. 2014). The reason for such self-correlation is the common presence of u_* in both variables—the ordinate σ_u/u_* and the the abscissa $\zeta = z/L$, where u_*^3 dictates the Obukhov length L.

Some previous studies (Pahlow et al. 2001; Juang et al. 2008) reported an increase of σ_u/u_* with ζ and this increase exhibits an approximate 1/3 scaling, which is indicative of possible artificial self-correlation. The forest experiments used here also show a similar 1/3 scaling behavior when σ_u/u_* is plotted against ζ, as illustrated in Fig. 11. Note again that σ_u itself reduces with increasing stability as shown in Fig. 8. Hence, to separate out the effect of stability on σ_u, the variation of σ_u with ζ from the model is shown for three different but prefixed u_* (i.e., no artificial self-correlation) in Fig. 12a. Figure 12b shows the variation of nondimensional σ_u/u_* with ζ and since the u_* is fixed (i.e., only the sensible heat flux varies), the curves show a self-similar behavior and decrease with increasing stability. Note the boundary layer height is also fixed in Fig. 12 for illustration though in reality δ will vary with increasing stability.

c. *Connection between shape of the stability functions and z-less stratification*

In Fig. 12 and also in Fig. 8, it can be observed that σ_u becomes independent of ζ after $\zeta \approx 2$, indicating that σ_u

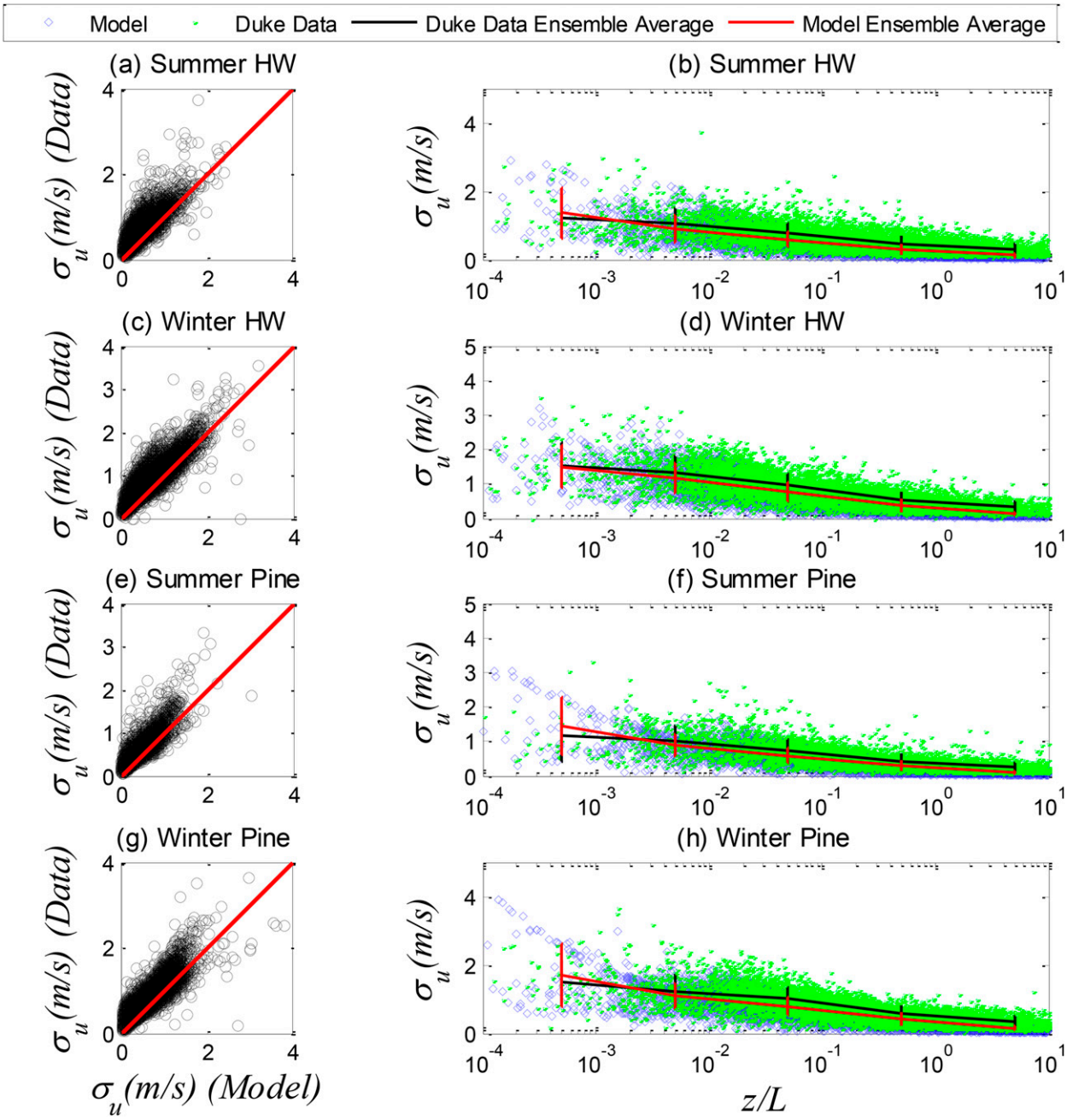

FIG. 10. (a),(c),(e),(g) Comparisons between measured and modeled σ_u using the formulation for zone II for the forest experiments. (b),(d),(f),(h) Variations of σ_u with ζ from the forest experiments and from the model using the formulation for zone II.

is no longer dependent on z when using the Kansas derived $\phi_m(\zeta)$ as noted earlier. This observation indicates the possible onset of z-less stratification and is commensurate with the same limit $\zeta \approx 2$ reported by other studies such as Olesen et al. (1984) and Kaimal and Finnigan (1994). Figure 13 shows the variation of σ_u with ζ for the second formulation (zone II) under high stability conditions. While the range of variation of σ_u is quite small, it also reaches z-less stratification reasonably at $\zeta \approx 10$ (the model results are extended to $\zeta = 10$ only for illustrating the near-leveling off when no other constraint is employed to suppress turbulence). As a result, the spectral budget model here predicts the z-less scaling for σ_u under high stability conditions. The "1/3" scaling of σ_u/u_* reported in some previous studies (Pahlow et al. 2001) may be the outcome of

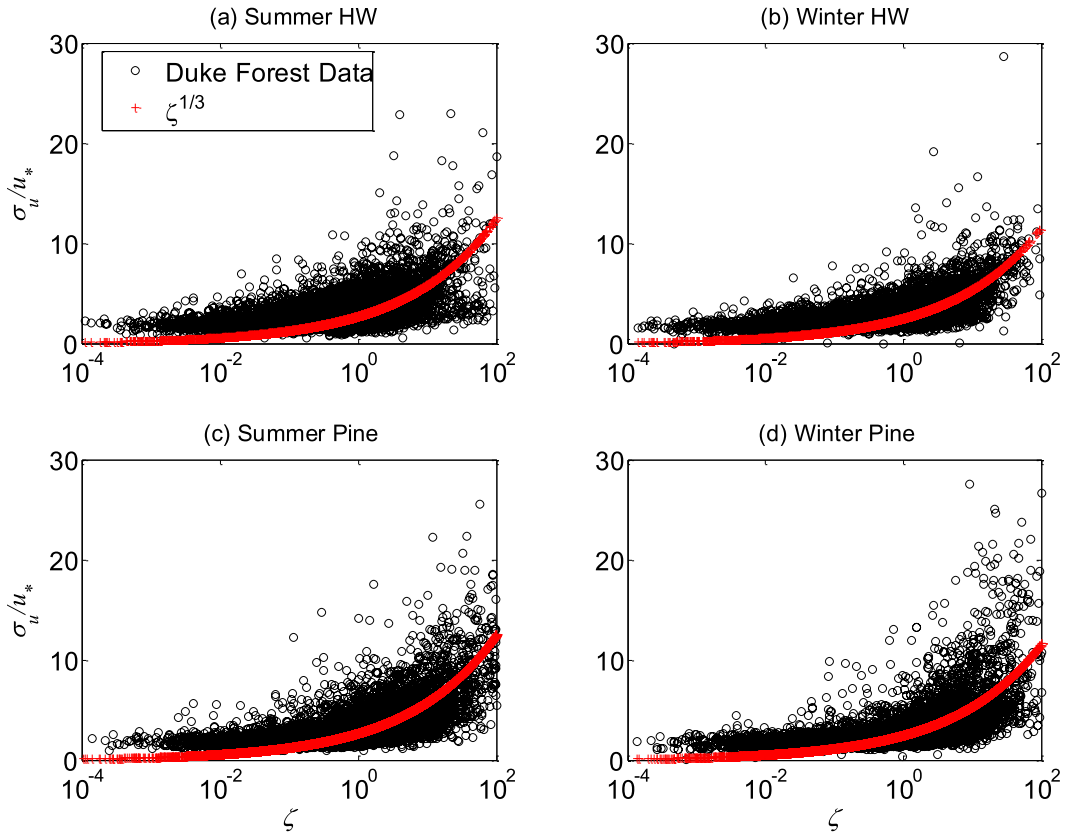

FIG. 11. Variations of σ_u/u_* with ζ from the forest experiments. The red line shows the $\zeta^{1/3}$ scaling as an indication of self-correlation.

self-correlation and cannot be used to argue against the existence of the z-less stratification in isolation of other metrics. However, it is to be noted that while the behavior of σ_u cannot be predicted from ϕ_m and ϕ_h alone, the variation of σ_u is heavily dependent on $\phi_m(\zeta)$ and $\phi_h(\zeta)$. Still, the choices of $\phi_m(\zeta)$ and $\phi_h(\zeta)$ are not ad hoc and are standard in the literature. MOST predicts an unbounded increase of $\phi_m(\zeta)$ and $\phi_h(\zeta)$ with ζ so they are not used beyond $\zeta > 2$. Nevertheless, a recent work by Chenge and Brutsaert (2005) provided alternative functional forms for $\phi_m(\zeta)$ and $\phi_h(\zeta)$ that level off after $\zeta = 1$. The effect of this variation on the onset of z-less scaling is discussed in appendix C. As foreshadowed by Eq. (37), the leveling off in $\phi_m(\zeta)$ precludes a z-less scaling, which is confirmed by detailed calculations shown in appendix C. Hence, the model results here establish a connection between the shape of the stability correction functions for mean velocity and temperature and z-less scaling in σ_u.

6. Conclusions

A spectral budget framework has been developed to describe the longitudinal turbulent intensity σ_u under stable atmospheric stratification. In presence of stable stratification, although turbulence is generated by mechanical processes, buoyancy effects counter mechanical effects and consequently reduce the turbulent intensity. Thus, in the spectral budget framework, the mechanical production term and the buoyant destruction term compete with each other. Two stability regimes are identified and separated at $\zeta = z/L \approx 0.1$. In the first regime ($\zeta \leq 0.1$), the resulting normalized longitudinal velocity variance is found to be consistent with the log law proposed by Townsend although the Townsend's coefficients are found to vary mildly with the atmospheric stability parameters. The second regime ($\zeta > 0.1$) results in a truncated spectrum exhibiting a $-5/3$ scaling even at low wavenumbers instead of a -1. Interestingly, the second regime formulation does not contain the boundary layer height. Thus, it can be concluded that at $\zeta > 0.1$, σ_u is not sensitive to the boundary layer height.

The model outcomes using the formulation for regime I are compared to data from a controlled laboratory experiment, a field campaign over a smooth lake surface, and two extensive datasets collected over tall vegetation canopies. The formulation for regime II is

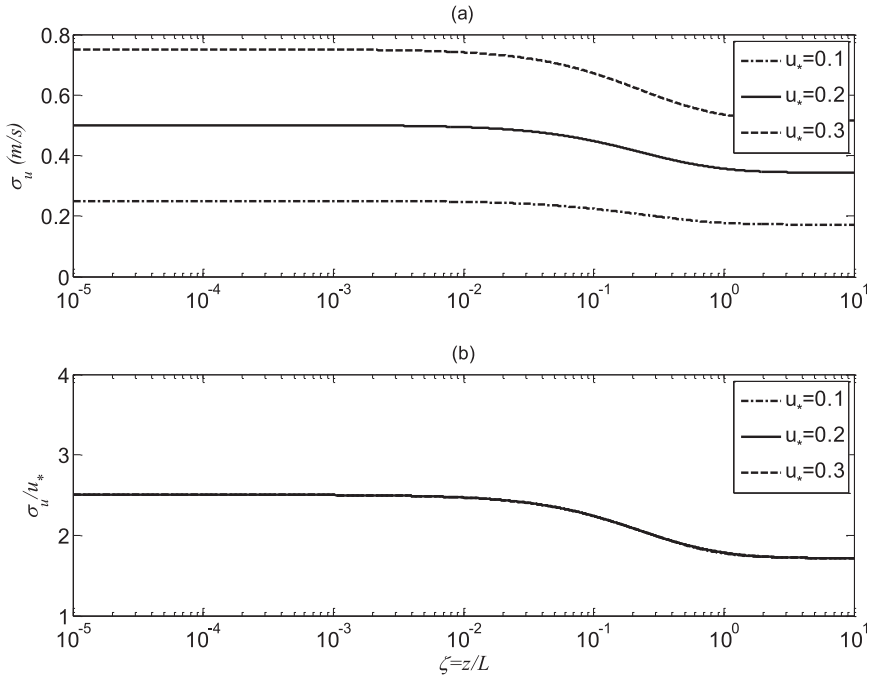

FIG. 12. Variations of (a) σ_u and (b) σ_u/u_* with ζ for three different but preset u_* from the model using the formulation for zone I. The flattened lines at $\zeta = 2$ indicate z-less stratification.

also compared with the field data over canopies. It is also found that σ_u decreases with increasing stability as expected. However, some previous studies had predicted an increase of σ_u/u_* with increasing stability parameter $\zeta = z/L$. This may be partly explained by the artificial self-correlation as a consequence of choosing common scaling variables in abscissa and ordinate. Hence, to separate out the effect of increasing stability on turbulent intensity, σ_u is deemed to be a more robust variable compared to σ_u/u_*. With this choice, the same data that show increasing trend of σ_u/u_* with z/L display a reduction of σ_u with increasing z/L, which is satisfactorily predicted by the model with zone I formulation. The modeled σ_u with a prefixed u_* flattens as z/L approaches 0 and recovers the correct neutral limit. The modeled σ_u also flattens and becomes asymptotic after $z/L = 2$. This result may signify that the model supports the existence of z-less stratification for a preset u_* and also correctly captures the limit $z/L = 2$ as the onset of z-less stratification when the Kansas stability correction functions for momentum and mean air temperature gradients are used. The second formulation as a limiting scenario for high stability regimes predicts an upper limit for the onset of z-less stratification after $\zeta \approx 2$. From an operational perspective, if the boundary layer height is not measured precisely, it can be calculated from a simple model and the predicted σ_u would not suffer much, because of the low sensitivity to δ (the order of magnitude is important, not the precise value). The proposed framework here brings together seemingly unrelated theories of turbulence such as Kolmogorov's hypothesis, Heisenberg's eddy viscosity, Townsend's hypothesis, and MOST scaling under a common framework. It also provides a physical basis for illustrating links between a number of well-established constants.

Acknowledgments. T.B. and G.K. acknowledge support from the National Science Foundation (NSF-EAR-134470,

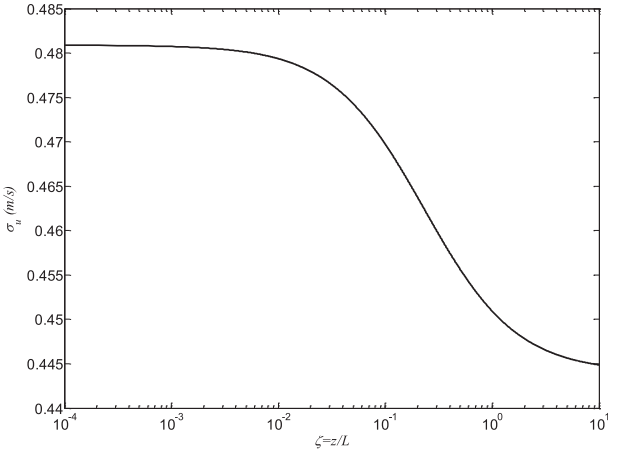

FIG. 13. Variations of σ_u with ζ from the model using the formulation for zone II.

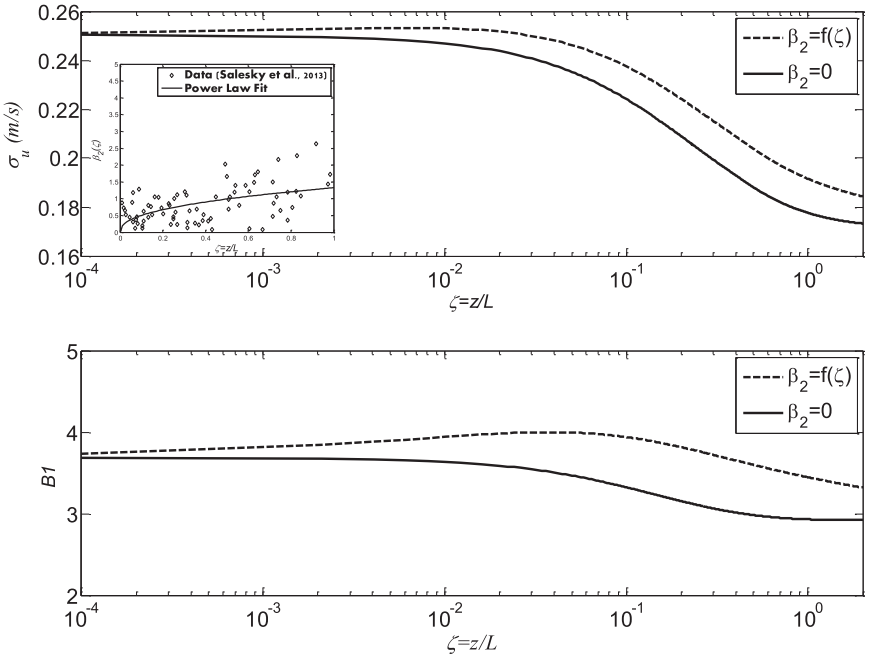

FIG. A1. First-order effects of a stability-dependent imbalance in the TKE budget. (top) σ_u computed using the formulation for zone I with a $\beta_2(\zeta)$ set to be zero (solid line) and a power-law function of ζ (dashed line). Here β_2 is computed by fitting a power law to the AHATS data compiled by Salesky et al. (2013) as shown in the inset. (bottom) The variation of the associated Townsend parameter B_1 with stability for the two approaches.

NSF-AGS-1102227) and the U.S. Department of Energy (DOE) through the office of Biological and Environmental Research (BER) Terrestrial Ecosystem Science (TES) Program (DE-SC0006967 and DE-SC0011461). DL acknowledges support from the NOAA (U.S. Department of Commerce) Grant NA08OAR4320752 and the Carbon Mitigation Initiative at Princeton University, sponsored by BP. The statements, findings, and conclusions are those of the authors and do not necessarily reflect the views of the NOAA, the U.S. Department of Commerce, or BP.

APPENDIX A

Effect of Imbalance in the TKE Budget

The first-order effect of a stability-dependent imbalance in the TKE budget is now explored. As discussed before, in stable conditions, there might be an imbalance between the production and dissipation terms indicating that the transport terms might be significant. In that case, the spectral budget should also contain terms arising out of Fourier transformation of those terms but it becomes overwhelmingly complicated. Instead, a simple first-order correction accounting for the imbalance is sought that can be perhaps encapsulated by the imbalance term $\beta_2(\zeta)$ in $\bar{\varepsilon}$. The stability variation of this term from the AHATS campaign is compiled by Salesky et al. (2013) and the data are fitted with a power law for the present work ($\beta_2 = 1.33\zeta^{0.42}$; see inset in Fig. A1). It is to be noted that the neutral limit of this term is zero and thus the formulation I is still valid. The only modification is in the Townsend coefficient B_1:

$$B_1 = \frac{3}{2}\frac{C_o}{\kappa^{2/3}}[\beta_2(\zeta) + \phi_m - \zeta]^{2/3}\gamma^{2/3} + 2c\gamma^2. \quad \text{(A1)}$$

Figure A1 shows the effect of this term. The top panel shows σ_u computed from the first formulation using a $\beta_2(\zeta)$ that is set to zero (original formulation, solid line) and is set to be a power-law function of ζ (dashed line). The bottom panel shows the variation of the associated Townsend parameter B_1 with stability for the two approaches. As can be observed, the formulation with the correction is slightly higher compared to the first formulation, but the difference is not highly significant.

APPENDIX B

Biases in the Comparison to Forest Data

The biases arising from using both formulation I and formulation II for the entire range of z/L are now

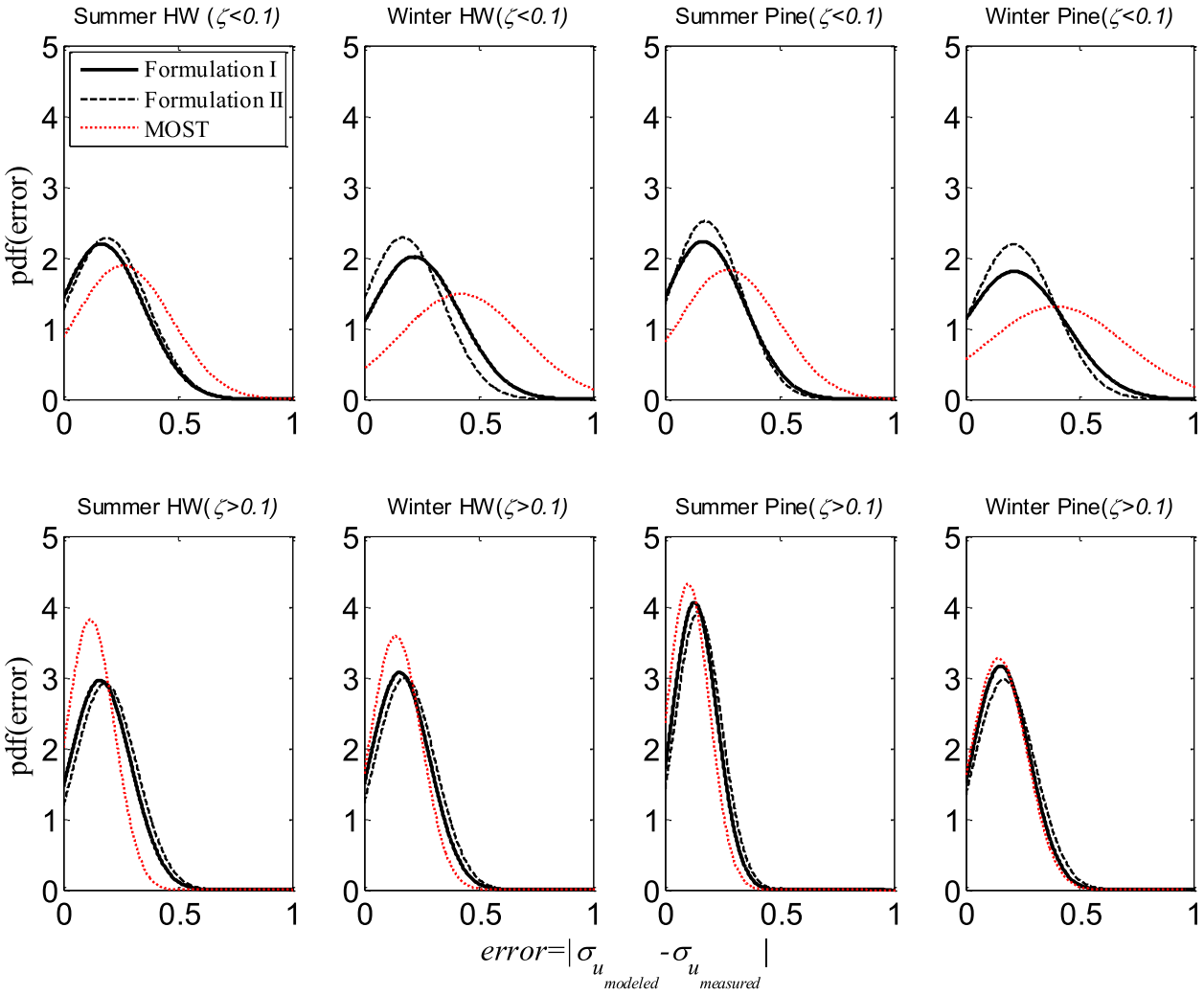

FIG. B1. Pdf of errors in the comparison between measured and modeled σ_u with the proposed formulations and MOST for the forest experiments. Black lines indicate the pdf of errors in the comparison with the formulation for zone I. Dashed black lines indicate the pdf of errors in the comparison with the formulation for zone II. Dotted red lines indicate the pdf of errors in comparison with MOST. (top) The regime of formulation I ($z/L < 0.1$) and (bottom) the regime for the formulation II ($z/L > 0.1$).

explored. Errors are calculated as the absolute value of the difference between the modeled and measured σ_u. Probability density functions (pdf) of errors are shown in Fig. B1. Black lines indicate the pdf of errors in the comparison with the formulation for zone I. Dashed black lines indicate the pdf of errors in the comparison with the formulation for zone II. Dotted red lines indicate the pdf of errors in comparison with MOST. The top row indicates the domain of formulation I ($z/L < 0.1$) and the bottom row indicates the domain for the formulation II ($z/L > 0.1$). As observed, most errors are concentrated on the lower side for our formulation, whereas for MOST, errors are more concentrated on the middle ranges, especially for lower stabilities. Note that for the forest data with $z/L > 0.1$, MOST ($\sigma_u = 2.5u_*$) performs well and compares reasonably with the proposed models. This finding perhaps proves the point that boundary layer height is not so significant at such stable conditions. Also, the stability dependence of σ_u is weak. Both of those results are consistent with the formulations for zone II.

APPENDIX C

Effect of Alternative Forms of $\phi_m(\zeta)$ and $\phi_h(\zeta)$

The effect of alternative forms of $\phi_m(\zeta)$ and $\phi_h(\zeta)$ are now discussed. The following forms were provided by Chenge and Brutsaert (2005):

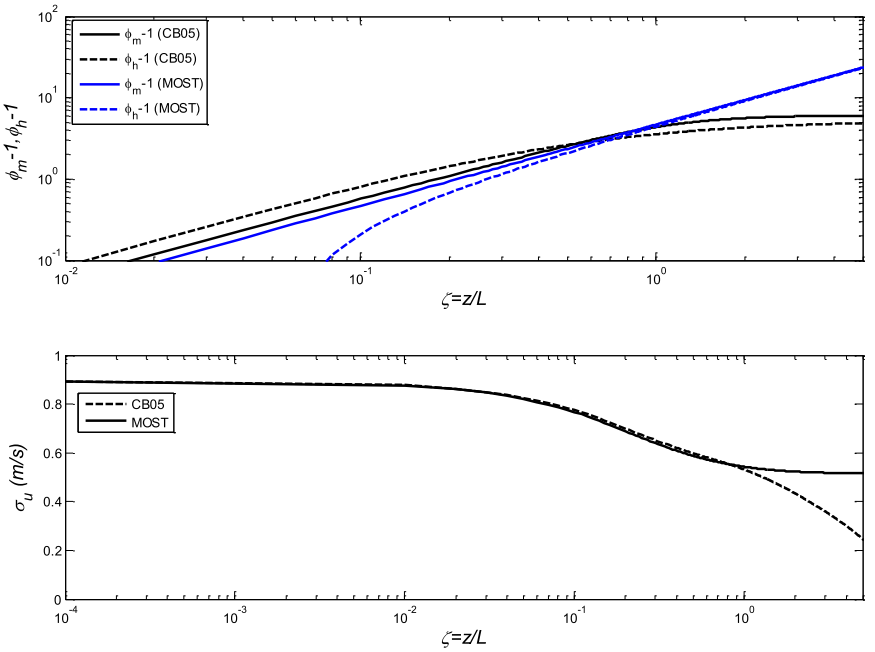

FIG. C1. (top) Correction functions prescribed by Chenge and Brutsaert (2005) (CB05) and MOST. (bottom) σ_u using CB05 and MOST.

$$\phi_m(\zeta) = 1 + a\left[\frac{\zeta + \zeta^b(1+\zeta^b)^{(1-b)/b}}{\zeta + (1+\zeta^b)^{1/b}}\right] \quad \text{and} \quad \text{(C1)}$$

$$\phi_h(\zeta) = 1 + c\left[\frac{\zeta + \zeta^d(1+\zeta^d)^{(1-d)/d}}{\zeta + (1+\zeta^d)^{1/d}}\right], \quad \text{(C2)}$$

where $a = 6.1$, $b = 2.5$, $c = 5.3$, and $d = 1.1$. Figure C1 shows these functions $\phi_m(\zeta) - 1$ and $\phi_h(\zeta) - 1$ in the top panel (black lines) along with traditional MOST forms (blue lines). The bottom panel of Fig. C1 shows a sample variation of σ_u computed using $\phi_m(\zeta)$ and $\phi_h(\zeta)$ both with MOST (solid line) and Eqs. (C1) and (C2) (dashed line). It is noted that σ_u does not flatten after $\zeta = 1$ (like MOST) but reduces further with these modified functions. Thus the onset of z-less stratification is further "delayed."

REFERENCES

Alfredsson, P. H., A. Segalini, and R. Örlü, 2011: A new scaling for the streamwise turbulence intensity in wall-bounded turbulent flows and what it tells us about the "outer" peak. *Phys. Fluids*, **23**, 041702, doi:10.1063/1.3581074.

Andreas, E. L, and B. B. Hicks, 2002: Comments on "Critical test of the validity of Monin–Obukhov similarity during convective conditions." *J. Atmos. Sci.*, **59**, 2605–2607, doi:10.1175/1520-0469(2002)059<2605:COCTOT>2.0.CO;2.

Arya, S., 1981: Parameterizing the height of the stable atmospheric boundary layer. *J. Appl. Meteor.*, **20**, 1192–1202, doi:10.1175/1520-0450(1981)020<1192:PTHOTS>2.0.CO;2.

Banerjee, T., and G. G. Katul, 2013: Logarithmic scaling in the longitudinal velocity variance explained by a spectral budget. *Phys. Fluids*, **25**, 125106, doi:10.1063/1.4837876.

——, ——, S. T. Salesky, and M. Chamecki, 2014: Revisiting the formulations for the logitudinal velocity variance in the unstable atmospheric surface layer. *Quart. J. Roy. Meteor. Soc.*, **141**, 1699–1711, doi:10.1002/qj.2472.

Basu, S., F. Porté-Agel, E. Foufoula-Georgiou, J.-F. Vinuesa, and M. Pahlow, 2006: Revisiting the local scaling hypothesis in stably stratified atmospheric boundary-layer turbulence: An integration of field and laboratory measurements with large-eddy simulations. *Bound.-Layer Meteor.*, **119**, 473–500, doi:10.1007/s10546-005-9036-2.

——, A. Ruiz-Columbié, J. Phillipson, and S. Harshan, 2010: Local scaling characteristics of Antarctic surface layer turbulence. *Cryosphere*, **4**, 325–331, doi:10.5194/tc-4-325-2010.

——, A. Holtslag, L. Caporaso, A. Riccio, and G.-J. Steeneveld, 2014: Observational support for the stability dependence of the bulk Richardson number across the stable boundary layer. *Bound.-Layer Meteor.*, **150**, 515–523, doi:10.1007/s10546-013-9878-y.

Bradshaw, P., 1978: Comments on "Horizontal velocity spectra in an unstable surface layer." *J. Atmos. Sci.*, **35**, 1768–1770, doi:10.1175/1520-0469(1978)035<1768:COVSIA>2.0.CO;2.

Businger, J. A., and A. M. Yaglom, 1971: Introduction to Obukhov's paper on turbulence in an atmosphere with a non-uniform temperature. *Bound.-Layer Meteor.*, **2**, 3–6, doi:10.1007/BF00718084.

Cai, X., G. Peng, X. Guo, and M. Leclerc, 2008: Evaluation of backward and forward Lagrangian footprint models in the surface layer. *Theor. Appl. Climatol.*, **93**, 207–223, doi:10.1007/s00704-007-0334-0.

Campos, J. G., O. C. Acevedo, J. Tota, and A. O. Manzi, 2009: On the temporal scale of the turbulent exchange of carbon dioxide

and energy above a tropical rain forest in Amazonia. *J. Geophys. Res.*, **114**, D08124, doi:10.1029/2008JD011240.

Canuto, V., Y. Cheng, A. Howard, and I. Esau, 2008: Stably stratified flows: A model with no Ri(cr). *J. Atmos. Sci.*, **65**, 2437–2447, doi:10.1175/2007JAS2470.1.

Caughey, S., 1977: Boundary-layer turbulence spectra in stable conditions. *Bound.-Layer Meteor.*, **11**, 3–14, doi:10.1007/BF00221819.

Cava, D., U. Giostra, M. Siqueira, and G. Katul, 2004: Organised motion and radiative perturbations in the nocturnal canopy sublayer above an even-aged pine forest. *Bound.-Layer Meteor.*, **112**, 129–157, doi:10.1023/B:BOUN.0000020160.28184.a0.

——, G. Katul, A. M. Sempreviva, U. Giostra, and A. Scrimieri, 2008: On the anomalous behaviour of scalar flux–variance similarity functions within the canopy sub-layer of a dense alpine forest. *Bound.-Layer Meteor.*, **128**, 33–57, doi:10.1007/s10546-008-9276-z.

Charuchittipan, D., and J. Wilson, 2009: Turbulent kinetic energy dissipation in the surface layer. *Bound.-Layer Meteor.*, **132**, 193–204, doi:10.1007/s10546-009-9399-x.

Chenge, Y., and W. Brutsaert, 2005: Flux-profile relationships for wind speed and temperature in the stable atmospheric boundary layer. *Bound.-Layer Meteor.*, **114**, 519–538, doi:10.1007/s10546-004-1425-4.

De Bruin, H. A. R., 1982: The energy balance of the Earth's surface: A practical approach. Ph.D. thesis, Wageningen Agricultural University, 186 pp.

Dyer, A. J., 1974: A review of flux-profile relationships. *Bound.-Layer Meteor.*, **7**, 363–372, doi:10.1007/BF00240838.

Edwards, N. R., and S. D. Mobbs, 1997: Observations of isolated wave-turbulence interactions in the stable atmospheric boundary layer. *Quart. J. Roy. Meteor. Soc.*, **123**, 561–584, doi:10.1002/qj.49712353903.

Einaudi, F., and J. Finnigan, 1981: The interaction between an internal gravity wave and the planetary boundary layer. Part I: The linear analysis. *Quart. J. Roy. Meteor. Soc.*, **107**, 793–806, doi:10.1002/qj.49710745404.

Finnigan, J., and F. Einaudi, 1981: The interaction between an internal gravity wave and the planetary boundary layer. Part II: Effect of the wave on the turbulence structure. *Quart. J. Roy. Meteor. Soc.*, **107**, 807–832, doi:10.1002/qj.49710745405.

——, ——, and D. Fua, 1984: The interaction between an internal gravity wave and turbulence in the stably-stratified nocturnal boundary layer. *J. Atmos. Sci.*, **41**, 2409–2436, doi:10.1175/1520-0469(1984)041<2409:TIBAIG>2.0.CO;2.

Grachev, A. A., E. L Andreas, C. W. Fairall, P. S. Guest, and P. O. G. Persson, 2013: The critical Richardson number and limits of applicability of local similarity theory in the stable boundary layer. *Bound.-Layer Meteor.*, **147**, 51–82, doi:10.1007/s10546-012-9771-0.

Hansen, K. S., R. J. Barthelmie, L. E. Jensen, and A. Sommer, 2012: The impact of turbulence intensity and atmospheric stability on power deficits due to wind turbine wakes at Horns Rev wind farm. *Wind Energy*, **15**, 183–196, doi:10.1002/we.512.

Hartogensis, O., and H. A. R. De Bruin, 2005: Monin–Obukhov similarity functions of the structure parameter of temperature and turbulent kinetic energy dissipation rate in the stable boundary layer. *Bound.-Layer Meteor.*, **116**, 253–276, doi:10.1007/s10546-004-2817-1.

Heisenberg, W., 1948: On the theory of statistical and isotropic turbulence. *Proc. Roy. Soc. London*, **195A**, 402–406, doi:10.1098/rspa.1948.0127.

Hicks, B. B., 1978: Some limitations of dimensional analysis and power laws. *Bound.-Layer Meteor.*, **14**, 567–569, doi:10.1007/BF00121895.

——, 1981: An examination of turbulence statistics in the surface boundary layer. *Bound.-Layer Meteor.*, **21**, 389–402, doi:10.1007/BF00119281.

Hinze, J., 1959: *Turbulence*. McGraw-Hill, 586 pp.

Högström, U., 1990: Analysis of turbulence structure in the surface layer with a modified similarity formulation for near neutral conditions. *J. Atmos. Sci.*, **47**, 1949–1972, doi:10.1175/1520-0469(1990)047<1949:AOTSIT>2.0.CO;2.

Hsieh, C.-I., and G. G. Katul, 2009: The Lagrangian stochastic model for estimating footprint and water vapor fluxes over inhomogeneous surfaces. *Int. J. Biometeor.*, **53**, 87–100, doi:10.1007/s00484-008-0193-0.

Huang, J., and E. Bou-Zeid, 2013: Turbulence and vertical fluxes in the stable atmospheric boundary layer. Part I: A large-eddy simulation study. *J. Atmos. Sci.*, **70**, 1513–1527, doi:10.1175/JAS-D-12-0167.1.

Hunt, J. C. R., J. C. Kaimal, and J. E. Gaynor, 1985: Some observations of turbulence structure in stable layers. *Quart. J. Roy. Meteor. Soc.*, **111**, 793–815, doi:10.1002/qj.49711146908.

Huwald, H., C. Higgins, M. Boldi, E. Bou-Zeid, M. Lehning, and M. Parlange, 2009: Albedo effect on radiative errors in air temperature measurements. *Water Resour. Res.*, **45**, W08431, doi:10.1029/2008WR007600.

Juang, J.-Y., G. G. Katul, M. B. Siqueira, P. C. Stoy, and H. R. McCarthy, 2008: Investigating a hierarchy of Eulerian closure models for scalar transfer inside forested canopies. *Bound.-Layer Meteor.*, **128**, 1–32, doi:10.1007/s10546-008-9273-2.

Kader, B., and A. Yaglom, 1990: Mean fields and fluctuation moments in unstably stratified turbulent boundary layers. *J. Fluid Mech.*, **212**, 637–662, doi:10.1017/S0022112090002129.

Kaimal, J. C., 1973: Turbulenece spectra, length scales and structure parameters in the stable surface layer. *Bound.-Layer Meteor.*, **4**, 289–309, doi:10.1007/BF02265239.

——, 1978: Horizontal velocity spectra in an unstable surface layer. *J. Atmos. Sci.*, **35**, 18–24, doi:10.1175/1520-0469(1978)035<0018:HVSIAU>2.0.CO;2.

——, and J. J. Finnigan, 1994: *Atmospheric Boundary Layer Flows: Their Structure and Measurement.* Oxford University Press, 289 pp.

——, J. C. Wyngaard, Y. Izumi, and O. R. Coté, 1972: Spectral characteristics of surface-layer turbulence. *Quart. J. Roy. Meteor. Soc.*, **98**, 563–589, doi:10.1002/qj.49709841707.

Katul, G. G., A. G. Konings, and A. Porporato, 2011: Mean velocity profile in a sheared and thermally stratified atmospheric boundary layer. *Phys. Rev. Lett.*, **107**, 268502, doi:10.1103/PhysRevLett.107.268502.

——, A. Porporato, and V. Nikora, 2012: Existence of k^{-1} power-law scaling in the equilibrium regions of wall-bounded turbulence explained by Heisenberg's eddy viscosity. *Phys. Rev.*, **86E**, 066311, doi:10.1103/PhysRevE.86.066311.

——, D. Li, M. Chamecki, and E. Bou-Zeid, 2013: Mean scalar concentration profile in a sheared and thermally stratified atmospheric surface layer. *Phys. Rev.*, **87E**, 023004, doi:10.1103/PhysRevE.87.023004.

——, A. Porporato, S. Shah, and E. Bou-Zeid, 2014: Two phenomenological constants explain similarity laws in stably stratified turbulence. *Phys. Rev.*, **89E**, 023007, doi:10.1103/PhysRevE.89.023007.

Kolmogorov, A. N., 1941: The local structure of turbulence in incompressible viscous fluid for very large Reynolds numbers. *Dokl. Akad. Nauk SSSR*, **30**, 299–303.

Launiainen, J., 1995: Derivation of the relationship between the Obukhov stability parameter and the bulk Richardson number for flux-profile studies. *Bound.-Layer Meteor.*, **76**, 165–179, doi:10.1007/BF00710895.

Leyi, Z., and H. Panofsky, 1983: Wind fluctuations in stable air at the boulder tower. *Bound.-Layer Meteor.*, **25**, 353–362, doi:10.1007/BF02041154.

Li, D., and E. Bou-Zeid, 2011: Coherent structures and the dissimilarity of turbulent transport of momentum and scalars in the unstable atmospheric surface layer. *Bound.-Layer Meteor.*, **140**, 243–262, doi:10.1007/s10546-011-9613-5.

——, ——, and H. De Bruin, 2012a: Monin–Obukhov similarity functions for the structure parameters of temperature and humidity. *Bound.-Layer Meteor.*, **145**, 45–67, doi:10.1007/s10546-011-9660-y.

——, G. G. Katul, and E. Bou-Zeid, 2012b: Mean velocity and temperature profiles in a sheared diabatic turbulent boundary layer. *Phys. Fluids*, **24**, 105105, doi:10.1063/1.4757660.

——, ——, and ——, 2015a: Turbulent energy spectra and cospectra of momentum and heat fluxes in the stable atmospheric surface layer. *Bound.-Layer Meteor.*, **157**, 1–21, doi:10.1007/s10546-015-0048-2.

——, ——, and S. S. Zilitinkevich, 2015b: Revisiting the turbulent Prandtl number in an idealized atmospheric surface layer. *J. Atmos. Sci.*, **72**, 2394–2410, doi:10.1175/JAS-D-14-0335.1.

Lumley, J., 1967: Similarity and the turbulent energy spectrum. *Phys. Fluids*, **10**, 855–858, doi:10.1063/1.1762200.

Mahrt, L., 1998: Nocturnal boundary-layer regimes. *Bound.-Layer Meteor.*, **88**, 255–278, doi:10.1023/A:1001171313493.

——, E. Moore, D. Vickers, and N. Jensen, 2001: Dependence of turbulent velocity variances on scale and stability. *Air Pollution Modeling and Its Application XIV*, S.-E. Gryning and F. A. Schiermeier, Eds., Springer, 437–444.

——, S. Richardson, N. Seaman, and D. Stauffer, 2012: Turbulence in the nocturnal boundary layer with light and variable winds. *Quart. J. Roy. Meteor. Soc.*, **138**, 1430–1439, doi:10.1002/qj.1884.

Marusic, I., J. P. Monty, M. Hultmark, and A. J. Smits, 2013: On the logarithmic region in wall turbulence. *J. Fluid Mech.*, **716**, R3, doi:10.1017/jfm.2012.511.

McKeon, B., 2013: Natural logarithms. *J. Fluid Mech.*, **718**, 1–4, doi:10.1017/jfm.2012.608.

Monin, A., and A. Obukhov, 1954: Basic laws of turbulent mixing in the surface layer of the atmosphere. *Tr. Akad. Nauk SSSR Geophiz. Inst.*, **24**, 163–187.

Nieuwstadt, F. T., 1984: The turbulent structure of the stable, nocturnal boundary layer. *J. Atmos. Sci.*, **41**, 2202–2216, doi:10.1175/1520-0469(1984)041<2202:TTSOTS>2.0.CO;2.

Ohya, Y., D. E. Neff, and R. N. Meroney, 1997: Turbulence structure in a stratified boundary layer under stable conditions. *Bound.-Layer Meteor.*, **83**, 139–162, doi:10.1023/A:1000205523873.

Olesen, H. R., S. E. Larsen, and J. Højstrup, 1984: Modelling velocity spectra in the lower part of the planetary boundary layer. *Bound.-Layer Meteor.*, **29**, 285–312, doi:10.1007/BF00119794.

Pahlow, M., M. B. Parlange, and F. Porté-Agel, 2001: On Monin–Obukhov similarity in the stable atmospheric boundary layer. *Bound.-Layer Meteor.*, **99**, 225–248, doi:10.1023/A:1018909000098.

Panchev, S., 1971: *Random Functions and Turbulence.* Pergamon Press, 443 pp.

Poggi, D., G. Katul, and J. Albertson, 2006: Scalar dispersion within a model canopy: Measurements and three-dimensional Lagrangian models. *Adv. Water Resour.*, **29**, 326–335, doi:10.1016/j.advwatres.2004.12.017.

Pope, S., 2000: *Turbulence Flows.* Cambridge University Press, 779 pp.

Rohr, J., E. Itsweire, K. Helland, and C. Van Atta, 1988: Growth and decay of turbulence in a stably stratified shear flow. *J. Fluid Mech.*, **195**, 77–111, doi:10.1017/S0022112088002332.

Salesky, S. T., G. G. Katul, and M. Chamecki, 2013: Buoyancy effects on the integral lengthscales and mean velocity profile in atmospheric surface layer flows. *Phys. Fluids*, **25**, 105101, doi:10.1063/1.4823747.

Smits, A. J., and I. Marusic, 2013: Wall-bounded turbulence. *Phys. Today*, **66**, 25–30, doi:10.1063/PT.3.2114.

Stevens, R. J., M. Wilczek, and C. Meneveau, 2014: Large-eddy simulation study of the logarithmic law for second and higher-order moments in turbulent wall-bounded flow. *J. Fluid Mech.*, **757**, 888–907, doi:10.1017/jfm.2014.510.

Stull, R. B., 1988: *An Introduction to Boundary Layer Meteorology*. Kluwer Academic, 666 pp.

Sukoriansky, S., and B. Galperin, 2013: An analytical theory of the buoyancy-Kolmogorov subrange transition in turbulent flows with stable stratification. *Philos. Trans. Roy. Soc. London*, **371A**, doi:10.1098/rsta.2012.0212.

——, ——, and V. Perov, 2006: A quasi-normal scale elimination model of turbulence and its application to stably stratified flows. *Nonlinear Processes Geophys.*, **13**, 9–22, doi:10.5194/npg-13-9-2006.

Townsend, A. A., 1976: *The Structure of Turbulent Shear Flow.* Cambridge University Press, 433 pp.

Vercauteren, N., E. Bou-Zeid, M. B. Parlange, U. Lemmin, H. Huwald, J. Selker, and C. Meneveau, 2008: Subgrid-scale dynamics for water vapor, heat, and momentum over a lake. *Bound.-Layer Meteor.*, **128**, 205–228, doi:10.1007/s10546-008-9287-9.

Weinstock, J., 1981: Energy dissipation rates of turbulence in the stable free atmosphere. *J. Atmos. Sci.*, **38**, 880–883, doi:10.1175/1520-0469(1981)038<0880:EDROTI>2.0.CO;2.

Wilson, J., 2008: Monin-Obukhov functions for standard deviations of velocity. *Bound.-Layer Meteor.*, **129**, 353–369, doi:10.1007/s10546-008-9319-5.

Wyngaard, J., and O. Coté, 1971: The budgets of turbulent kinetic energy and temperature variance in the atmospheric surface layer. *J. Atmos. Sci.*, **28**, 190–201, doi:10.1175/1520-0469(1971)028<0190:TBOTKE>2.0.CO;2.

Yang, D., C. Meneveau, and L. Shen, 2014: Large-eddy simulation of offshore wind farm. *Phys. Fluids*, **26**, 025101, doi:10.1063/1.4863096.

Zilitinkevich, S., 1972: On the determination of the height of the Ekman boundary layer. *Bound.-Layer Meteor.*, **3**, 141–145, doi:10.1007/BF02033914.

——, and P. Calanca, 2000: An extended similarity theory for the stably stratified atmospheric surface layer. *Quart. J. Roy. Meteor. Soc.*, **126**, 1913–1923, doi:10.1256/smsqj.56617.

——, T. Elperin, N. Kleeorin, I. Rogachevskii, and I. Esau, 2013: A hierarchy of energy- and flux-budget (EFB) turbulence closure models for stably-stratified geophysical flows. *Bound.-Layer Meteor.*, **146**, 341–373, doi:10.1007/s10546-012-9768-8.